

## ABSTRACT

Title of Thesis:       **OBSERVER-BASED FEEDBACK  
CONTROL FOR STABILIZATION  
OF COLLECTIVE MOTION**

Seth Ochse Napora, Master of Science, 2011

Thesis directed by:   Professor Derek A. Paley  
Department of Aerospace Engineering

Multi-vehicle control has applications in weather monitoring and ocean sampling. Previous work in this field has produced theoretically justified algorithms for stabilization of parallel and circular motions of self-propelled Newtonian particles using measurements of relative position and relative velocity. This paper describes an observer-based feedback control algorithm for stabilization of parallel and circular motions using measurements of relative position only. The algorithm utilizes information about vehicle dynamics and turning rates to estimate relative velocity. Theoretical justification is provided for the vehicle model, and numerical simulations suggest that the algorithm extends to a three-dimensional rigid body model. The algorithm has been implemented on a laboratory-scale underwater vehicle testbed, and we describe the results of experimental validation in the University of Maryland's Neutral Buoyancy Research Facility.

OBSERVER-BASED FEEDBACK CONTROL FOR  
STABILIZATION OF COLLECTIVE MOTION

by

Seth Ochse Napora

Thesis submitted to the Faculty of the Graduate School of the  
University of Maryland, College Park in partial fulfillment  
of the requirements for the degree of  
Master of Science  
2011

Advisory Committee:  
Professor Derek A. Paley, Chair  
Professor Robert M. Sanner  
Professor David Akin

© Copyright by  
Seth Ochse Napora  
2011

## Dedication

I would like to dedicate this work to my brother and parents. They have always been there and provided me with help and support.

## Acknowledgments

I would like to take this opportunity to thank everyone that has helped me throughout my academic career. During my studies at the University of Maryland, I have thoroughly enjoyed working in the Collective Dynamics and Control Laboratory focusing on the design, development, and implementation of an autonomous underwater vehicle testbed. This research would not have been possible without the assistance of Dr. Derek A. Paley, my mentor. His thorough advice and insightful suggestions have proven to be invaluable to my research. Additionally, I would also like to specifically recognize Levi DeVries and Nitin Sydney. Their consistent involvement in the submarine testing over the years has helped produce informative and useful results which have been noted throughout this paper. Also, Rochelle Mellish, Cammy Peterson, and Sachit Butail have been helpful in providing theoretical input. Finally, I am grateful to the members of the Collective Dynamics and Control Laboratory and the Space Systems Laboratory who have always taken the time out of their day to support me in my research.

# Table of Contents

List of Tables	v
List of Figures	v
1 Introduction & Chapter Outline	1
1.1 Introduction . . . . .	1
1.2 Chapter Outline . . . . .	3
2 Background	5
2.1 Self-Propelled Vehicle Model with First-Order Steering Control . . . . .	5
2.2 Self-Propelled Vehicle Model with Second-Order Steering Control . . . . .	7
3 Theoretical Results	12
3.1 Dynamic Model of Relative Orientation . . . . .	12
3.2 Velocity Estimation . . . . .	15
3.3 Observer-Based Feedback Control . . . . .	18
4 Simulation Results	26
4.1 Six Degree of Freedom Submarine Model . . . . .	26
4.2 Numerical Integration of Submarine Model . . . . .	28
4.3 Simulated Cooperative Control Algorithms . . . . .	30
4.3.1 Parallel & Circular Control . . . . .	30
4.3.2 Observer-Based Feedback Control . . . . .	35
5 Experimental Results	39
5.1 Underwater-Vehicle Testbed . . . . .	39
5.2 Qualisys Motion Capture System . . . . .	44
5.3 Experimental Results of the Underwater Vehicle Testbed . . . . .	46
5.3.1 Virtual Vehicle Experiments . . . . .	46
5.3.2 Multi-Vehicle Experiments . . . . .	47
5.3.3 Observer-Based Feedback Control Experiments . . . . .	53
6 Conclusion & Future Work	56
6.1 Conclusion . . . . .	56
6.2 Future Work . . . . .	56
Bibliography	59

## List of Tables

4.1	Physical miniature submarine properties . . . . .	27
-----	---	----

## List of Figures

2.1	Collective motions of the self-propelled vehicle model . . . . .	6
2.2	A simulation of five self-propelled vehicles performing the parallel control law using a proportional turning rate controller. . . . .	8
2.3	A simulation of five self-propelled vehicles performing the circular control law using a proportional turning rate controller with $\omega_0 = 0.25$ . . . . .	10
3.1	Vectors utilized in dynamic model . . . . .	13
3.2	Estimator gain relationship . . . . .	18
3.3	A simulation of five self-propelled vehicles performing the parallel control law using the observer-based feedback control algorithm. . . . .	23
3.4	A simulation of five self-propelled vehicles performing the circular control law using the observer-based feedback control algorithm with $\omega_0 = 0.25$ . . . . .	25
4.1	Free-body diagram of submarine model . . . . .	27
4.2	A simulation of five submarine models performing the parallel control law . . . . .	32
4.3	A simulation of five submarine models performing the circular control law . . . . .	34
4.4	Simulations of five submarine models performing the observer-based feedback control algorithm in which they exhibit oscillatory behavior . . . . .	36
4.5	A simulation of five submarine models performing the scheduled parallel control law . . . . .	37
4.6	A simulation of five submarine models performing the circular control law with small alignment gain and $\omega_0 = 0.25$ . . . . .	38
5.1	Miniature submarine models of the U.S.S. Albacore that comprise the underwater vehicle testbed . . . . .	40
5.2	Wiring diagram for remote operation . . . . .	41
5.3	Wiring diagram for autonomous operation . . . . .	42
5.4	Pseudocode running onboard the arduIMU+ board . . . . .	43
5.5	Qualisys Motion Capture System . . . . .	44
5.6	Control architecture for the underwater vehicle testbed. . . . .	45
5.7	Experimental test runs of a single submarine performing the parallel control law with a virtual vehicle. . . . .	48
5.8	Experimental test runs of a single submarine performing the circular control law with a virtual vehicle. . . . .	49
5.9	Experimental test runs of two submarines performing the parallel control law. . . . .	51

5.10	Experimental test runs of two submarines performing the circular control law. . . . .	52
5.11	Experimental test run of two submarines performing the parallel control law using the observer-based feedback control algorithm. . . . .	54
5.12	Experimental test run of two submarines performing the circular control law using the observer-based feedback control algorithm. . . . .	54

# Chapter 1

## Introduction & Chapter Outline

### 1.1 Introduction

Motivation for pursuing coordinated, collective motion of autonomous vehicles comes from the desire to estimate rapidly evolving spatiotemporal processes using mobile sensor networks. For example, a collection of UAV's performing environmental sampling can further the understanding of the rapid intensification of tropical cyclones [11] and transmission of airborne pathogens [24, 25]. A collection of vehicles is better suited to sample these environmental phenomena than an individual platform because the collection can rapidly perform measurements over larger areas. Similarly, sampling of oceanic processes for greater sonar performance prediction can benefit from multi-vehicle cooperation [10, 17]. Other applications include underwater minesweeping [4] and boundary tracking [6] for oil spills and algae growth.

Prior work in the field of collective motion has produced many control algorithms for vehicles modeled as self-propelled particles. In [21], theoretically justified control laws for this model are provided which stabilize synchronized, balanced, and circular formations. The authors in [15] and [16] built upon these control laws and adapt them to function in the presence of a spatially and temporally varying flow-field. The authors in [12] provide a second-order steering control for a self-propelled

particle model using backstepping as an alternate to proportional control. The authors in [3] examine collective motion via pursuit dynamics where a leader particle performed a behavior and the others pursued the leader.

A challenge to achieving collective motion is the stabilization of moving formations with limited information. In [23], a flocking behavior of agents is described whereby only a certain number of agents are informed of the desired behavior. Flocking motion is still possible under this restriction, as also described in [22], which discussed a self-propelled particle system with limited communication between agents. Information can also be limited by sensing capabilities. In these cases, other approaches must be taken to determine the missing information. In [2], limited sensing was overcome using sliding-mode estimators to achieve formation tracking.

Additional research into cooperative control involves the experimental validation of the proposed control algorithm. Validation can be achieved through a variety of platforms ranging from aircraft to submersibles. The researchers in [20] designed a cost effective ground platform capable of self-assembly while the authors of [9] utilized a fin-actuated platform to stabilize parallel and balanced formations. The authors in [10] and [25] utilized vehicles capable of waypoint navigation to perform the desired behavior.

In current work here, parallel and circular motions are studied utilizing a vehicle model with second-order steering control. Both formation control algorithms require that a vehicle is aware of the relative velocity orientation of any vehicle in the group. Instead, we assume that each vehicle is capable of sensing the relative position

of other vehicles as well as its own turning rate. The theoretical contributions of this paper are to present theoretically justified methods for (1) estimating the velocity of one vehicle relative to another vehicle and (2) utilizing that estimate in an observer-based feedback control algorithm to stabilize parallel and circular formations in a self-propelled vehicle model with second-order rotational dynamics.

We also describe a three-dimensional rigid body model alongside simulations that illustrate the performance of the estimation and control algorithms onboard a more realistic model. The higher fidelity model is designed to mimic the behavior of the underwater vehicles that comprise our laboratory scale testbed. The laboratory facility allows for validation of the control algorithms along with the ability to easily regulate the platform's sensing capabilities, which allows us to simulate sensing limitations.

## 1.2 Chapter Outline

The outline for the paper is as follows. In Chapter 2, a kinematic and dynamic vehicle model are described along with theoretically justified cooperative control laws for parallel and circular motion. Chapter 3 derives an observer-based feedback control algorithm to stabilize these collective behaviors utilizing relative position and vehicle turning rate to estimate the relative velocity orientation required for control. Chapter 4 describes a three-dimensional rigid body submarine model developed to simulate the cooperative control algorithms on a higher fidelity model. This model mimics the behavior of miniature radio-controlled submarines used in Chapter 5 to

experimentally validate these algorithms. Chapter 6 summarizes the results of this paper and future work.

## Chapter 2

### Background

In our study of collective motion, we consider parallel and circular formations as building blocks for more complex motion. These cooperative motions have been achieved in [21] using a particle model to represent each vehicle in a group. We describe that model here, along with a vehicle model that includes second-order rotational dynamics. For each model, we include a description of control algorithms for stabilizing parallel and circular formations.

#### 2.1 Self-Propelled Vehicle Model with First-Order Steering Control

A dynamic model that has been used to design collective motion [21] is a self-propelled vehicle model with first-order steering control also known as a self-propelled particle model. This model assumes that each agent moves in the plane at a constant speed, often assumed to be one. The position of vehicle  $k$  is  $\mathbf{r}_k = [x_k \ y_k]^T$ , and the orientation of its (planar, unit) velocity is  $\theta_k$ . The steering control,  $\nu_k$ , is applied to the heading rate allowing the vehicle to change course as indicated below:

$$\begin{aligned} \dot{x}_k &= \cos \theta_k \\ \dot{y}_k &= \sin \theta_k \\ \dot{\theta}_k &= \nu_k, \end{aligned} \tag{2.1}$$

where  $k$  represents the  $k$ th vehicle in a group of size  $N$ . Collective control laws have been designed for this model resulting in parallel and circular formations [21].

The parallel formation is achieved when each vehicle obtains the same velocity orientation. The following control achieves this motion with all-to-all communication [21]:

$$\nu_k = -\frac{K}{N} \sum_{j=1}^N \sin(\theta_j - \theta_k) \triangleq \alpha_k(\boldsymbol{\theta}_k), \quad (2.2)$$

where  $\boldsymbol{\theta}_k = [\theta_1 - \theta_k, \dots, \theta_N - \theta_k]$ . Note that the absolute orientations of the other vehicles' velocities are not required for control  $\nu_k$ , only the relative orientations. The choice of control gain  $K$  influences the convergence speed of the formation as well as the formation type. Choosing  $K < 0$  in (2.2) produces straight-line motion where all the vehicle trajectories are parallel [21]. Choosing  $K > 0$  yields balanced motion; this behavior occurs when the sum of all vehicles' velocities is equal to zero. These motions are illustrated in Fig. 2.1.

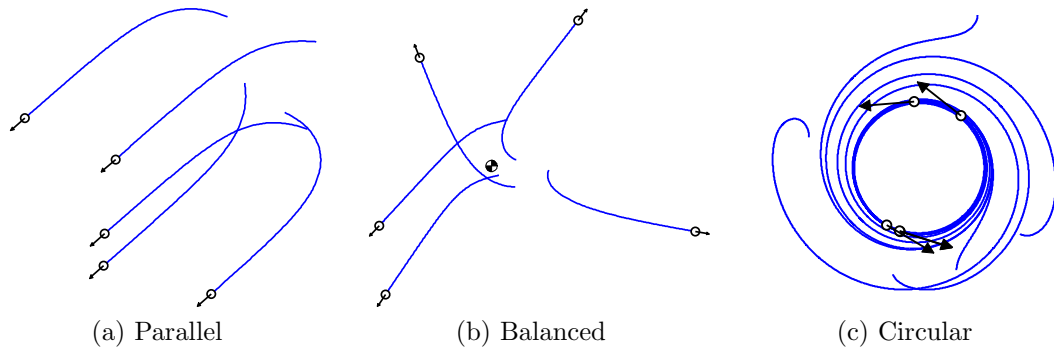


Figure 2.1: Collective motions of the self-propelled vehicle model

A circular formation is achieved when each vehicle's turning rate and center of rotation are identical to the rest of the group. The center of rotation  $\mathbf{c}_k$ , is defined

in Cartesian notation with respect to an inertial frame  $\mathcal{I}$  as

$$\mathbf{c}_k = [\mathbf{r}_k]_{\mathcal{I}} + \omega_0^{-1} \begin{bmatrix} -\sin \theta_k \\ \cos \theta_k \end{bmatrix}_{\mathcal{I}}, \quad (2.3)$$

where  $|\omega_0|^{-1}$  is the circle's radius. Using the center of rotation, the following control expressed in matrix notation produces a circular formation with all-to-all communication [21]

$$\nu_k = \omega_0 (1 + K \mathcal{P}_k \mathbf{c} \dot{\mathbf{r}}_k) \triangleq \gamma_k(\mathbf{R}_k, \boldsymbol{\theta}_k), \quad (2.4)$$

where  $\mathbf{c} = [\mathbf{c}_1, \dots, \mathbf{c}_N]^T$ ,  $\mathbf{R}_k = [r_1 - r_k, \dots, r_N - r_k]^T$ , and  $K > 0$ .  $\mathcal{P}_k$  is the  $k$ th row of the projector matrix  $\mathcal{P} = I_{N \times N} - \frac{1}{N} \mathbf{1} \mathbf{1}^T$ , where  $\mathbf{1} = [1, \dots, 1]^T \in \mathbb{R}^N$ . This formation is also illustrated in Fig. 2.1.

Note that the circular control law for vehicle  $k$  can be expressed in terms of relative velocity orientations,  $\boldsymbol{\theta}_k$ , and relative positions,  $\mathbf{R}_k$ , expressed as components in a path reference frame (see Section 3.1).

## 2.2 Self-Propelled Vehicle Model with Second-Order Steering

### Control

The first-order vehicle model is useful for studying various group behaviors, but may not adequately represent the rotational dynamics of an actual vehicle. Instead of controlling the heading rate to change direction, a typical vehicle applies

a moment to control the rotational acceleration. Under this assumption, each vehicle has the following dynamics:

$$\begin{aligned}
 \dot{x}_k &= \cos \theta_k \\
 \dot{y}_k &= \sin \theta_k \\
 \dot{\theta}_k &= \omega_k \\
 \dot{\omega}_k &= u_k.
 \end{aligned} \tag{2.5}$$

The control laws (2.2) and (2.4) derived for the vehicle model with first-order steering control can be extended to the vehicle model with second-order steering control via a proportional controller that drives the desired turning rate to that of the first-order model's control law. The parallel formation for this model becomes [12],

$$u_k = K_p(\alpha_k(\boldsymbol{\theta}_k) - \omega_k), \tag{2.6}$$

where  $\alpha_k(\boldsymbol{\theta}_k)$  is defined in (2.2) and  $K_p > 0$ . A five vehicle simulation of this control law is illustrated in Fig. 2.2.

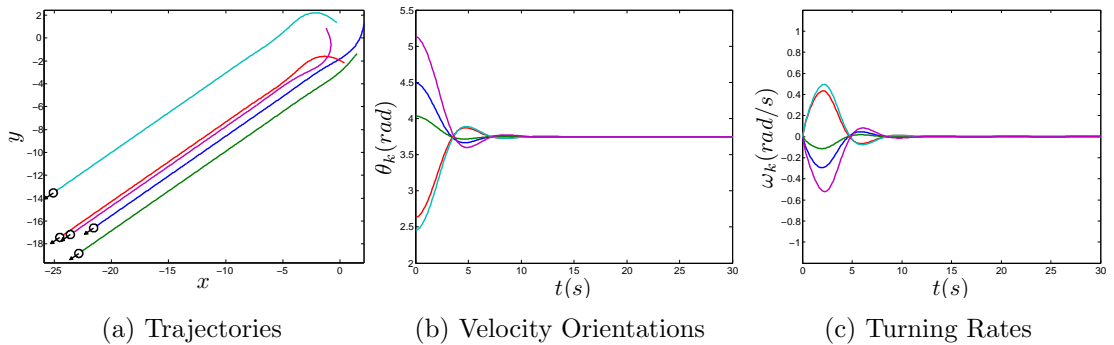


Figure 2.2: A simulation of five self-propelled vehicles performing the parallel control law using a proportional turning rate controller. Each vehicle is given a random initial position and velocity orientation;  $K = -1$  and  $K_p = 1$ .

**Theorem 1.** *The vehicle model (2.5) with control (2.6), where  $\alpha_k(\boldsymbol{\theta}_k)$  is defined in*

(2.2), stabilizes the set of parallel formations in which  $\theta_k = \theta_j$  for all pairs  $k, j$  and  $\omega_k = 0$  for all  $k$ .

*Proof.* Begin by examining the second-order rotational dynamics of a single vehicle implementing the parallel control law

$$\begin{aligned}\dot{\theta}_k &= \omega_k \\ \dot{\omega}_k &= K_p(K[-\sin \theta_k \ \cos \theta_k]p_\theta - \omega_k)\end{aligned}\tag{2.7}$$

where  $K < 0$ ,  $K_p > 0$ , and  $p_\theta = \frac{1}{N} \sum_{k=1}^N \hat{\mathbf{r}}_k$ . These dynamics can be expanded to the entire system of  $N$  vehicles using vector notation as

$$\begin{aligned}\dot{\boldsymbol{\theta}} &= \boldsymbol{\omega} \\ \dot{\boldsymbol{\omega}} &= K_p(K(\nabla U)^T - \boldsymbol{\omega})\end{aligned}\tag{2.8}$$

where  $U(\boldsymbol{\theta}) = \frac{1}{2}\|p_\theta\|^2$ ,  $\boldsymbol{\theta} = [\theta_1, \dots, \theta_N]^T$ , and  $\boldsymbol{\omega} = [\omega_1, \dots, \omega_N]^T$ . Choosing the Lyapunov function

$$V(\boldsymbol{\theta}, \boldsymbol{\omega}) = \frac{1}{2}\boldsymbol{\omega}^T \boldsymbol{\omega} - K_p K U(\boldsymbol{\theta}) \geq 0,\tag{2.9}$$

yields the following derivative with respect to time

$$\begin{aligned}\dot{V} &= \dot{\boldsymbol{\omega}}^T \boldsymbol{\omega} - K_p K \nabla U \dot{\boldsymbol{\theta}} \\ &= K_p(K \nabla U - \boldsymbol{\omega}^T) \boldsymbol{\omega} - K_p K \nabla U \boldsymbol{\omega} \\ &= -K_p \boldsymbol{\omega}^T \boldsymbol{\omega}.\end{aligned}\tag{2.10}$$

According to the invariance principle, solutions converge to the largest invari-

ant set in which  $\dot{V} = 0$ , i.e., the set  $\Lambda = \{\omega_k \equiv 0, \forall k\}$ . In  $\Lambda$ ,  $\boldsymbol{\omega} = \dot{\boldsymbol{\omega}} = 0$ , which implies  $\nabla U = 0$ . Therefore,  $\Lambda$  contains the critical points of  $U(\boldsymbol{\theta})$  which include parallel, balanced, and unbalanced configurations. Only the set of parallel formations is stable for  $K < 0$  [21].  $\square$

Similarly, circular motion can be achieved with the second-order steering model using the following control law [12]

$$u_k = K_p(\gamma_k(\mathbf{R}_k, \boldsymbol{\theta}_k) - \omega_k), \quad (2.11)$$

where  $\gamma_k(\mathbf{R}_k, \boldsymbol{\theta}_k)$  is defined in (2.4) and  $K_p > 0$ . Simulation of this control algorithm is displayed in Fig. 2.3.

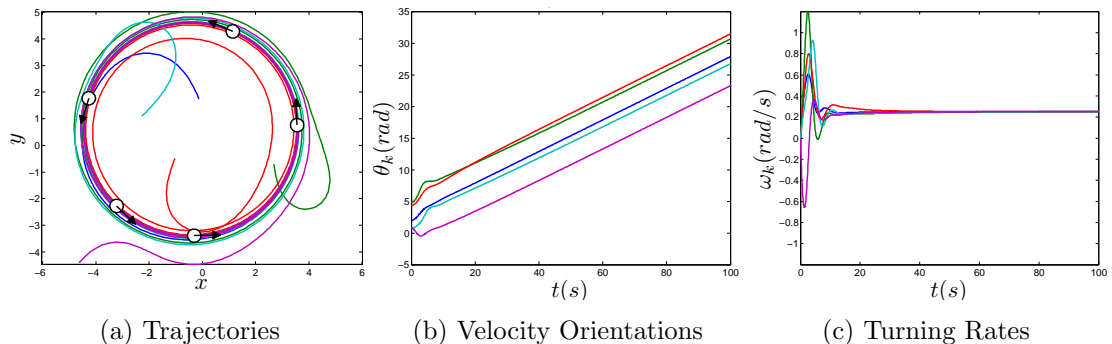


Figure 2.3: A simulation of five self-propelled vehicles performing the circular control law using a proportional turning rate controller with  $\omega_0 = 0.25$ . Each vehicle is given a random initial position and velocity orientation;  $K = 1$  and  $K_p = 1$ .

**Theorem 2.** *The vehicle model (2.5) with control (2.11), where  $\gamma_k(\mathbf{R}_k, \boldsymbol{\theta}_k)$  is defined in (2.4), stabilizes the set of circular formations in which  $\mathbf{c}_k = \mathbf{c}_j$  for all pairs  $k, j$  and  $\omega_k = \omega_0$  for all  $k$ .*

*Proof.* Consider the following composite Lyapunov function

$$V = \frac{K_p K \omega_0^2}{2} \text{trace}(\mathbf{c}^T \mathcal{P} \mathbf{c}) + \frac{1}{2} \sum_{k=1}^N (\omega_k - \omega_0)^2 \quad (2.12)$$

where  $\mathbf{c} = [\mathbf{c}_1, \dots, \mathbf{c}_N]^T$ ,  $K_p > 0$ ,  $K > 0$ , and  $\mathcal{P}$  is the projector matrix. Taking the derivative with respect to time yields

$$\begin{aligned} \dot{V} &= \sum_{k=1}^N K_p K \omega_0^2 \mathcal{P}_k \mathbf{c} \dot{\mathbf{r}}_k (1 - \omega_0^{-1} \omega_k) + (\omega_k - \omega_0) \dot{\omega}_k \\ \dot{V} &= \sum_{k=1}^N K_p K \omega_0 \mathcal{P}_k \mathbf{c} \dot{\mathbf{r}}_k (\omega_0 - \omega_k) - K_p (\omega_k - \omega_0)^2 \\ &\quad + K_p K \omega_0 \mathcal{P}_k \mathbf{c} \dot{\mathbf{r}}_k (\omega_k - \omega_0) \\ \dot{V} &= -K_p \sum_{k=1}^N (\omega_k - \omega_0)^2 \leq 0. \end{aligned} \quad (2.13)$$

According to the invariance principle, solutions converge to the largest invariant set in which  $\dot{V} = 0$ , i.e., the set  $\Lambda = \{\omega_k \equiv \omega_0, \forall k\}$ . In  $\Lambda$ ,  $\omega_k = \omega_0$  and  $\dot{\omega}_k = 0$ , which implies that each vehicle is constantly rotating at  $\omega_0$ . Based on (2.4), this constant rotational control occurs only when  $\mathcal{P}_k \mathbf{c} [1 \ 1]^T = 0 \ \forall k$ , i.e., each vehicle is traveling about the same circle.  $\square$

Theorems 1 and 2 ensure that the proportional controller stabilizes both parallel and circular formations on vehicle models with second-order steering control. With assurance that our control design is stable, the next step is to reduce the information required to perform these collective behaviors by examining the vehicle dynamics.

## Chapter 3

### Theoretical Results

As previously mentioned, parallel and circular motion have been achieved on vehicle models with first- and second-order steering control. These models assume that each vehicle is aware of the relative position and relative velocity orientation of other vehicles in the group. Here, we assume knowledge of relative position and turning rate only, and design an observer to estimate the relative velocity. Though we assume all-to-all communication, the extension to a limited communication topology is possible [22].

#### 3.1 Dynamic Model of Relative Orientation

Without loss of generality, we begin by examining a pair of vehicles  $j$  and  $k$ . Fig. 3.1 shows vehicles  $j$  and  $k$  in an inertial frame,  $\mathcal{I}$ . Each vehicle's position relative to the origin is represented by the vectors  $\mathbf{r}_j$  and  $\mathbf{r}_k$ , respectively, while the vector between the vehicles is represented by  $\mathbf{r}_{j/k} = \mathbf{r}_j - \mathbf{r}_k$ .

An inertial-frame representation is not necessarily known to each vehicle. Rather, vehicle  $k$  views the world from its own path frame  $\mathcal{B}_k = (k, \mathbf{x}_k, \mathbf{y}_k, \mathbf{z}_k)$  which rotates and translates with the vehicle itself. Unit vector  $\mathbf{x}_k$  is aligned with  $\dot{\mathbf{r}}_k$  as shown in Fig. 3.1 and  $\mathbf{y}_k = \mathbf{z}_k \times \mathbf{x}_k$ , where  $\mathbf{z}_k$  is out of the page. We express  $\mathbf{r}_{j/k}$  as components in frame  $\mathcal{B}_k$  as  $\mathbf{r}_{j/k} = x_{j/k}\mathbf{x}_k + y_{j/k}\mathbf{y}_k$ .

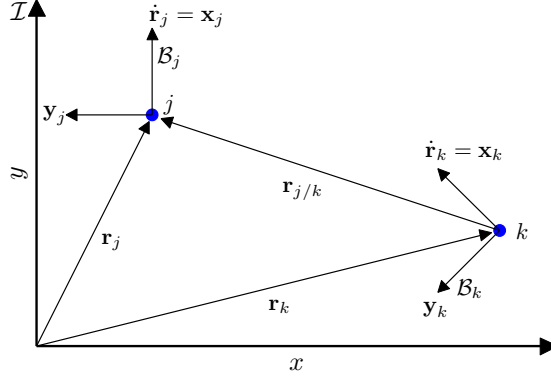


Figure 3.1: Vectors utilized in dynamic model

We begin by considering the inertial kinematics of  $j$  relative to  $k$ . Taking the derivative of  $\mathbf{r}_{j/k}$  with respect to the inertial frame and expressing the result in matrix notation with respect to frame  $\mathcal{I}$  yields

$$\begin{aligned}
 [{}^{\mathcal{I}}\mathbf{v}_{j/k}]_{\mathcal{I}} &= \left[ \frac{{}^{\mathcal{I}}d}{dt} \mathbf{r}_{j/k} \right]_{\mathcal{I}} = [\dot{\mathbf{r}}_j - \dot{\mathbf{r}}_k]_{\mathcal{I}} \\
 &= \begin{bmatrix} \cos \theta_j - \cos \theta_k \\ \sin \theta_j - \sin \theta_k \end{bmatrix}_{\mathcal{I}}.
 \end{aligned} \tag{3.1}$$

In this equation,  ${}^{\mathcal{I}}\mathbf{v}_{j/k}$  represents the velocity of vehicle  $j$  with respect to  $k$  in the inertial frame. The subscript  $\mathcal{I}$  refers to the coordinate system in which this quantity is expressed. For example,  $[{}^{\mathcal{I}}\mathbf{v}_{j/k}]_{\mathcal{I}}$  means that the inertial velocity of vehicle  $j$  with respect to vehicle  $k$  is expressed as vector components in the inertial frame,  $\mathcal{I}$ .

The inertial kinematics do not contain the relative orientation,  $\theta_j - \theta_k$ , which is needed to implement controllers (2.2) and (2.4). To obtain the relative orientation, we rewrite the inertial velocity in vehicle  $k$ 's path frame. The angular velocity of  $\mathcal{B}_k$  with respect to  $\mathcal{I}$  is  ${}^{\mathcal{I}}\boldsymbol{\omega}^{\mathcal{B}_k} = \omega_k \mathbf{z}_k$ . The velocity in the inertial frame can be

expressed as components in frame  $\mathcal{B}_k$ , using a  $2 \times 2$  rotation matrix  $R$  to rotate by  $-\theta_k$ :

$$\begin{aligned}
[\mathcal{I}\mathbf{v}_{j/k}]_{\mathcal{B}_k} &= R(-\theta_k) [\mathcal{I}\mathbf{v}_{j/k}]_{\mathcal{I}} \\
&= \begin{bmatrix} \cos(\theta_k) & \sin(\theta_k) \\ -\sin(\theta_k) & \cos(\theta_k) \end{bmatrix} \begin{bmatrix} \cos \theta_j - \cos \theta_k \\ \sin \theta_j - \sin \theta_k \end{bmatrix}_{\mathcal{I}} \\
&= \begin{bmatrix} \cos(\theta_j - \theta_k) - 1 \\ \sin(\theta_j - \theta_k) \end{bmatrix}_{\mathcal{B}_k}.
\end{aligned} \tag{3.2}$$

Although the resulting matrix contains the desired relative orientation, the term on the left is not directly measurable from the path frame. It can be related to the path frame velocity,  ${}^{\mathcal{B}_k}\mathbf{v}_{j/k}$ , using the transport equation [7]:

$$\frac{\mathcal{I}d}{dt}(\mathbf{r}_{j/k}) = \frac{{}^{\mathcal{B}_k}d}{dt}(\mathbf{r}_{j/k}) + \mathcal{I}\boldsymbol{\omega}^{\mathcal{B}_k} \times \mathbf{r}_{j/k}. \tag{3.3}$$

In matrix notation,

$$[\mathcal{I}\mathbf{v}_{j/k}]_{\mathcal{B}_k} = [{}^{\mathcal{B}_k}\mathbf{v}_{j/k}]_{\mathcal{B}_k} + [\boldsymbol{\omega}_k \mathbf{z}_k \times \mathbf{r}_{j/k}]_{\mathcal{B}_k}. \tag{3.4}$$

Using  $\mathbf{r}_{j/k} = x_{j/k}\mathbf{x}_k + y_{j/k}\mathbf{y}_k$  and  $\frac{{}^{\mathcal{B}_k}d}{dt}(\mathbf{r}_{j/k}) = s_{j/k}\mathbf{x}_k + v_{j/k}\mathbf{y}_k$  yields

$$\begin{bmatrix} \cos(\theta_j - \theta_k) - 1 \\ \sin(\theta_j - \theta_k) \end{bmatrix}_{\mathcal{B}_k} = \begin{bmatrix} s_{j/k} \\ v_{j/k} \end{bmatrix}_{\mathcal{B}_k} + \omega_k \begin{bmatrix} -y_{j/k} \\ x_{j/k} \end{bmatrix}_{\mathcal{B}_k}. \tag{3.5}$$

Solving for  $\theta_j - \theta_k$  yields

$$\theta_j - \theta_k = \arctan \left( \frac{v_{j/k} + \omega_k x_{j/k}}{1 + s_{j/k} - \omega_k y_{j/k}} \right). \quad (3.6)$$

Using relationship (3.6), calculating vehicle  $j$ 's velocity orientation relative to  $k$  requires knowledge of  $k$ 's turning rate as well as the position and velocity of vehicle  $j$  with respect to  $k$ . Assuming that the relative position,  $\mathbf{r}_{j/k}$ , and turning rate,  $\omega_k$ , are measured, each vehicle can estimate the relative velocity,  ${}^{\mathcal{B}_k}\mathbf{v}_{j/k}$ , in the path frame,  $\mathcal{B}_k$ , using the estimator described next.

### 3.2 Velocity Estimation

Consider the case where vehicle  $k$  is estimating the relative velocity of vehicle  $j$  in frame  $\mathcal{B}_k$ . In this case, let  $\hat{\mathbf{r}}_{j/k} = \hat{x}_{j/k}\mathbf{x}_k + \hat{y}_{j/k}\mathbf{y}_k$  and  ${}^{\mathcal{B}_k}\hat{\mathbf{v}}_{j/k} = \hat{s}_{j/k}\mathbf{x}_k + \hat{v}_{j/k}\mathbf{y}_k$  be the position and velocity estimates, respectively. Also, let  $\Delta\mathbf{r}_{j/k} \triangleq \hat{\mathbf{r}}_{j/k} - \mathbf{r}_{j/k}$  and  $\Delta{}^{\mathcal{B}_k}\mathbf{v}_{j/k} \triangleq {}^{\mathcal{B}_k}\hat{\mathbf{v}}_{j/k} - {}^{\mathcal{B}_k}\mathbf{v}_{j/k}$  represent the estimation errors for position and velocity. Note that we estimate the velocity of vehicle  $j$  with respect to vehicle  $k$  in frame  $\mathcal{B}_k$ . Choosing the estimator dynamics

$$\begin{aligned} {}^{\mathcal{B}_k}\frac{d}{dt}(\hat{\mathbf{r}}_{j/k}) &= -K_1\Delta\mathbf{r}_{j/k} + {}^{\mathcal{B}_k}\hat{\mathbf{v}}_{j/k} \\ {}^{\mathcal{B}_k}\frac{d}{dt}(\hat{\mathbf{v}}_{j/k}) &= -K_2\Delta\mathbf{r}_{j/k}, \end{aligned} \quad (3.7)$$

where  $K_1 > 0$  and  $K_2 > 0$ , yields the following error dynamics:

$$\underbrace{\mathcal{B}_k \frac{d}{dt} \begin{bmatrix} \Delta \mathbf{r}_{j/k} \\ \Delta \mathcal{B}_k \mathbf{v}_{j/k} \end{bmatrix}}_{\triangleq \dot{\mathbf{e}}_{j/k}} = \underbrace{\begin{bmatrix} -K_1 & 1 \\ -K_2 & 0 \end{bmatrix}}_{\triangleq A} \underbrace{\begin{bmatrix} \Delta \mathbf{r}_{j/k} \\ \Delta \mathcal{B}_k \mathbf{v}_{j/k} \end{bmatrix}}_{\triangleq \mathbf{e}_{j/k}} + \underbrace{\begin{bmatrix} 0 \\ -\mathcal{B}_k \mathbf{a}_{j/k} \end{bmatrix}}_{\triangleq \mathbf{g}_{j/k}(t)}. \quad (3.8)$$

Observe that the estimator is a linear system of the form  $\dot{\mathbf{e}}_{j/k} = A\mathbf{e}_{j/k} + \mathbf{g}_{j/k}(t)$ , where  $\mathbf{g}_{j/k}(t)$  is a time-varying perturbation.

Representing the equations in vector notation is useful in studying the stability of the system, but the vehicle model with second-order steering control (2.5) and the relative orientation relationship (3.6) utilize a Cartesian coordinate system with respect to the frame  $\mathcal{B}_k$ . To be consistent, we rewrite (3.7) as

$$\begin{aligned} \dot{\hat{x}}_{j/k} &= -K_1 \Delta x_{j/k} + \hat{s}_{j/k} \\ \dot{\hat{y}}_{j/k} &= -K_1 \Delta y_{j/k} + \hat{v}_{j/k} \\ \dot{\hat{s}}_{j/k} &= -K_2 \Delta x_{j/k} \\ \dot{\hat{v}}_{j/k} &= -K_2 \Delta y_{j/k}, \end{aligned} \quad (3.9)$$

where  $\Delta x_{j/k} \triangleq \hat{x}_{j/k} - x_{j/k}$  and  $\Delta y_{j/k} \triangleq \hat{y}_{j/k} - y_{j/k}$ .  $\hat{x}_{j/k}$  and  $\hat{y}_{j/k}$  represent the position estimates, and  $\hat{s}_{j/k}$  and  $\hat{v}_{j/k}$  represent the relative velocity estimates in frame  $\mathcal{B}_k$ .

The perturbation  $\mathbf{g}_{j/k}(t)$  is, in general, not bounded, but can be made arbitrarily small using an appropriate choice of gains described next.

**Lemma 3.** *The error in the velocity estimation due to perturbation  $\mathbf{g}_{j/k}(t)$  defined*

in (3.8), is proportional to the positive quantity

$$\epsilon \triangleq \frac{K_1^2 + K_2 + 1}{K_1 K_2}. \quad (3.10)$$

*Proof.* Consider the following Lyapunov function

$$V = \mathbf{e}_{j/k}^T P \mathbf{e}_{j/k} \quad (3.11)$$

where  $\mathbf{e}_{j/k} \triangleq [\Delta x_{j/k} \quad \mathcal{B}_k \frac{d}{dt} \Delta x_{j/k} \quad \Delta y_{j/k} \quad \mathcal{B}_k \frac{d}{dt} \Delta y_{j/k}]^T$ . The matrix  $P$  is chosen by solving the Lyapunov equation

$$PA + A^T P = -Q \quad (3.12)$$

where  $Q \in \mathbb{R}^{4 \times 4}$  is the identity matrix. For this system,

$$P = I_{2 \times 2} \otimes \begin{bmatrix} \frac{K_2 + 1}{2K_1} & -\frac{1}{2} \\ -\frac{1}{2} & \frac{\epsilon}{2} \end{bmatrix}. \quad (3.13)$$

Taking the derivative with respect to time yields

$$\dot{V} = -\mathbf{e}_{j/k}^T Q \mathbf{e}_{j/k} + \mathcal{B}_k \mathbf{a}_{j/k}^T (\Delta \mathbf{r}_{j/k} - \epsilon \Delta \mathcal{B}_k \mathbf{v}_{j/k}). \quad (3.14)$$

The estimator assumes that the relative position is known; therefore, the error in the position estimate is negligible. As a result, (3.14) ensures  $\dot{V} \leq 0$  for  $\|\mathbf{e}_{j/k}\| \geq b$ , where  $b$  is proportional to  $\epsilon \|\mathbf{g}_{j/k}(t)\|_{\mathcal{L}}$ .  $\square$

We have not identified an analytic method for optimally choosing gains  $K_1$  and  $K_2$ ; however, the quantity  $\epsilon$  defined in (3.10) can be minimized by choosing  $K_2 \gg K_1 \gg 1$ . A plot of this relationship is illustrated in Fig. 3.2.

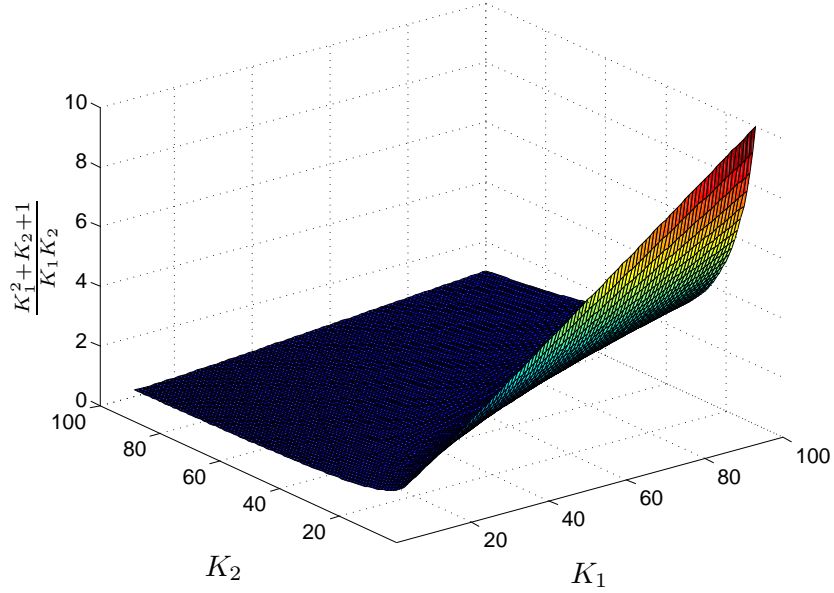


Figure 3.2: Estimator gain relationship

### 3.3 Observer-Based Feedback Control

Let's now consider a system comprised of  $N$  vehicles with second-order steering control (2.5). Each vehicle utilizes the estimator (3.9) to determine the relative velocities of the other vehicles. These estimates are then used to calculate the relative orientations of the vehicles using (3.6). Finally, each vehicle implements the desired control algorithm using the estimated relative orientations. The state-space representation of the combined system is:

$$\begin{aligned}
\dot{x}_k &= \cos(\theta_k) \\
\dot{y}_k &= \sin(\theta_k) \\
\dot{\theta}_k &= \omega_k \\
\dot{\omega}_k &= K_p(\hat{\nu}_k - \omega_k) \\
\dot{\hat{x}}_{j/k} &= -K_1\Delta x_{j/k} + \hat{s}_{j/k} \\
\dot{\hat{y}}_{j/k} &= -K_1\Delta y_{j/k} + \hat{\nu}_{j/k} \\
\dot{\hat{s}}_{j/k} &= -K_2\Delta x_{j/k} \\
\dot{\hat{\nu}}_{j/k} &= -K_2\Delta y_{j/k},
\end{aligned} \tag{3.15}$$

with  $k, j = 1, \dots, N$  and  $\hat{\nu}_k$  represents the desired control law.

Let

$$\widehat{\theta_j - \theta_k} = \arctan\left(\frac{\hat{\nu}_{j/k} + \omega_k \hat{x}_{j/k}}{1 + \hat{s}_{j/k} - \omega_k \hat{y}_{j/k}}\right) \tag{3.16}$$

and  $\hat{\boldsymbol{\theta}}_k = [\widehat{\theta_1 - \theta_k}, \dots, \widehat{\theta_N - \theta_k}]$ . Note that the combination of the control law and estimator establish the perturbation in (3.8) as vanishing [8] because vehicles in the desired formation do not move relative to the body frame,  $\mathcal{B}_k$ . If a vehicle remains stationary in frame  $\mathcal{B}_k$ , then  ${}^{\mathcal{B}_k}\mathbf{v}_{j/k} = {}^{\mathcal{B}_k}\mathbf{a}_{j/k} = 0$ .

For a parallel formation,  $\hat{\nu}_k$  in (3.15) is replaced by  $\alpha_k(\boldsymbol{\theta}_k)$  given in (2.2). Noting that the parallel control law is a summation of sine terms and the relative orientation calculation uses an inverse tangent, the control law can be simplified using trigonometric identities to

$$\alpha_k(\hat{\boldsymbol{\theta}}_k) = -\frac{K}{N} \sum_{j=1}^N \frac{\hat{\nu}_{j/k} + \omega_k \hat{x}_{j/k}}{\sqrt{(\hat{\nu}_{j/k} + \omega_k \hat{x}_{j/k})^2 + (1 + \hat{s}_{j/k} - \omega_k \hat{y}_{j/k})^2}}. \tag{3.17}$$

Implementation of the circular control law is achieved the same way using  $\hat{\nu}_k = \gamma_k(\mathbf{R}_k, \hat{\boldsymbol{\theta}}_k)$  where  $\gamma_k(\mathbf{R}_k, \hat{\boldsymbol{\theta}}_k)$  is given in (2.4). Note that the relative orientation in this algorithm is used to calculate the centers of rotation (2.3) in vehicle  $k$ 's path frame.

**Theorem 4.** *Choosing the control  $\nu_k = \alpha_k(\hat{\boldsymbol{\theta}}_k)$  defined in (2.2) ensures that, along solutions of (3.15),  $\mathbf{z} = [\boldsymbol{\omega}^T \ \mathbf{e}^T]^T$  is bounded by a quantity proportional to  $\epsilon$  given in (3.10).*

*Proof.* Consider the following composite Lyapunov function

$$V = \frac{1}{2}\boldsymbol{\omega}^T\boldsymbol{\omega} - K_p KU(\boldsymbol{\theta}) + \mathbf{e}^T(I_{N^2 \times N^2} \otimes P)\mathbf{e} \geq 0 \quad (3.18)$$

where  $K < 0$ ,  $K_p > 0$ ,  $\boldsymbol{\omega} = [\omega_1, \dots, \omega_N]^T$ , and  $N$  is the number of vehicles.  $\mathbf{e}$  is a  $4N^2 \times 1$  matrix of estimator errors given by

$$\mathbf{e} \triangleq \begin{bmatrix} \mathbf{e}_{1/1} & \mathbf{e}_{1/2} & \dots & \mathbf{e}_{1/N} & \mathbf{e}_{2/1} & \dots & \mathbf{e}_{N/N} \end{bmatrix}^T, \quad (3.19)$$

where  $\mathbf{e}_{j/k} \triangleq [\Delta x_{j/k} \quad \frac{B_k d}{dt} \Delta x_{j/k} \quad \Delta y_{j/k} \quad \frac{B_k d}{dt} \Delta y_{j/k}]$ . The matrix  $P$  is chosen by solving the Lyapunov equation,  $PA + A^T P = -Q$  where  $Q \in \mathbb{R}^{4 \times 4}$  is the identity matrix. For this system,

$$P = I_{2 \times 2} \otimes \begin{bmatrix} \frac{K_2+1}{2K_1} & -\frac{1}{2} \\ -\frac{1}{2} & \frac{\epsilon}{2} \end{bmatrix}, \quad (3.20)$$

where  $\epsilon$  is defined in (3.10). Taking the derivative with respect to time yields

$$\dot{V} = -K_p \boldsymbol{\omega}^T \boldsymbol{\omega} - \mathbf{e}^T (I_{N^2 \times N^2} \otimes Q) \mathbf{e} - \mathbf{1}^T (I_{N^2 \times N^2} \otimes B) (I_{2 \times 2} \otimes C) \mathbf{e}, \quad (3.21)$$

where  $I$  is the identity matrix,  $\mathbf{1} = [1, \dots, 1]^T \in \mathbb{R}^{4N^2}$ ,

$$B = I_{2 \times 2} \otimes \begin{bmatrix} -1 & 0 \\ 0 & \epsilon \end{bmatrix}, \quad (3.22)$$

and  $C$  is a  $2N^2 \times 2N^2$  diagonal matrix with diagonal

$$\left[ \mathcal{B}_k \mathbf{a}_{1/1} \quad \mathcal{B}_k \mathbf{a}_{1/1} \quad \mathcal{B}_k \mathbf{a}_{1/2} \quad \mathcal{B}_k \mathbf{a}_{1/2} \quad \dots \quad \mathcal{B}_k \mathbf{a}_{1/N} \quad \mathcal{B}_k \mathbf{a}_{1/N} \quad \dots \quad \mathcal{B}_k \mathbf{a}_{N/N} \quad \mathcal{B}_k \mathbf{a}_{N/N} \right]^T. \quad (3.23)$$

A change of coordinates is used to simplify (3.21) by letting

$$\mathbf{z} = \begin{bmatrix} \boldsymbol{\omega} \\ \mathbf{e} \end{bmatrix}, \quad \dot{\mathbf{z}} = \mathbf{z}^T \underbrace{\begin{bmatrix} K_p(I_{N \times N}) & 0 \\ 0 & I_{4N^2 \times 4N^2} \end{bmatrix}}_{\triangleq D} \mathbf{z}, \quad (3.24)$$

which yields

$$\dot{V} = -\mathbf{z}^T D \mathbf{z} - \mathbf{1}^T (I_{N^2 \times N^2} \otimes B) (I_{2 \times 2} \otimes C) \mathbf{e}. \quad (3.25)$$

Note that the second term can be rewritten as the following double summation

$$\sum_{k=1}^N \sum_{j=1}^N \mathcal{B}_k \mathbf{a}_{j/k}^T (\Delta \mathbf{r}_{j/k} - \epsilon \Delta^{\mathcal{B}_k} \mathbf{v}_{j/k}), \quad (3.26)$$

where  $\Delta \mathbf{r}_{j/k}$  is the position error and  $\Delta^{\mathcal{B}_k} \mathbf{v}_{j/k}$  is the velocity error. In the context of the problem, we assume that the relative position is measured. Therefore, in steady-state,  $\Delta \mathbf{r}_{j/k}$  is proportional to the measurement noise, which we ignore. This simplification allows the function of gains to be pulled outside of the double summation and used to scale this term in the Lyapunov derivative. Under this simplification,  $\dot{V} \leq 0$  when

$$\mathbf{z}^T D \mathbf{z} > \epsilon \sum_{k=1}^N \sum_{j=1}^N \|\mathcal{B}_k \mathbf{a}_{j/k}^T \Delta^{\mathcal{B}_k} \mathbf{v}_{j/k}\|. \quad (3.27)$$

Hence, solutions that lie outside the bound  $\mathbf{z}^T D \mathbf{z} = \epsilon \sum_{k=1}^N \sum_{j=1}^N \|\mathcal{B}_k \mathbf{a}_{j/k}^T \Delta^{\mathcal{B}_k} \mathbf{v}_{j/k}\|$ , will approach this boundary. Once inside, solutions will remain there because  $\dot{V} < 0$  in the region outside of the boundary.  $\square$

In this stability condition, we have some authority over  $\epsilon$  through our choice of estimator gains. Making  $\epsilon$  small reduces the ultimate bound on  $z$ , allowing vehicles to approach arbitrarily close to the parallel formation. Simulated results of the parallel formation are displayed in Fig. 3.3.

**Theorem 5.** *Choosing the control  $\nu_k = \gamma_k(\hat{\boldsymbol{\theta}}_k, \mathbf{R}_k)$  defined in (2.4) guarantees that along solutions of (3.15),  $\mathbf{z} = [(\boldsymbol{\omega}^T - \omega_0 \mathbf{1}^T) \ \mathbf{e}^T]^T$  is bounded by a quantity proportional to  $\epsilon$  given in (3.10).*

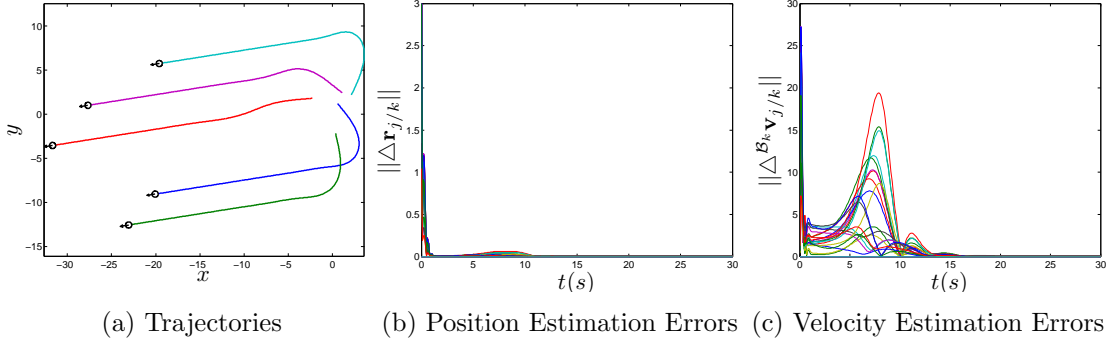


Figure 3.3: A simulation of five self-propelled vehicles performing the parallel control law using the observer-based feedback control algorithm. Each vehicle is given a random initial position and velocity;  $K = -1$ ,  $K_p = 1$ ,  $K_1 = 10$ , and  $K_2 = 100$ .

*Proof.* Consider the following composite Lyapunov function

$$V = \mathbf{e}^T (I_{N^2 \times N^2} \otimes P) \mathbf{e} + \frac{K_p K \omega_0^2}{2} \text{trace}(\mathbf{c}^T \mathcal{P} \mathbf{c}) + \frac{1}{2} \sum_{k=1}^N (\omega_k - \omega_0)^2 \quad (3.28)$$

where  $\mathbf{c} = [\mathbf{c}_1, \dots, \mathbf{c}_N]^T$ ,  $K_p > 0$ ,  $K > 0$ , and  $\mathcal{P}$  is the projector matrix. The vector  $\mathbf{e}$  and matrix  $P$  are defined in (3.19) and (3.20), respectively. Taking the derivative with respect to time yields

$$\begin{aligned} \dot{V} &= \mathbf{e}^T (I_{N^2 \times N^2} \otimes Q) \mathbf{e} - \mathbf{1}^T (I_{N^2 \times N^2} \otimes B) (I_{2 \times 2} \otimes C) \mathbf{e} \\ &\quad - K_p (\boldsymbol{\omega} - \omega_0 \mathbf{1})^T (\boldsymbol{\omega} - \omega_0 \mathbf{1}), \end{aligned} \quad (3.29)$$

where  $\boldsymbol{\omega} = [\omega_1, \dots, \omega_N]$  and  $Q \in \mathbb{R}^{4 \times 4}$  is the identity matrix. The matrix  $B$  is defined in (3.22). A change of coordinates is used to simplify (3.29) by letting

$$\mathbf{z} = \begin{bmatrix} \boldsymbol{\omega} - \omega_0 \mathbf{1} \\ \mathbf{e} \end{bmatrix}, \quad \dot{\mathbf{z}} = \mathbf{z}^T D \mathbf{z}, \quad (3.30)$$

where  $D$  is defined in (3.24), which yields

$$\dot{V} = -\mathbf{z}^T D \mathbf{z} - \mathbf{1}^T (I_{N^2 \times N^2} \otimes B) (I_{2 \times 2} \otimes C) \mathbf{e}. \quad (3.31)$$

Note that the second term can be rewritten as the following double summation

$$\sum_{k=1}^N \sum_{j=1}^N \mathcal{B}_k \mathbf{a}_{j/k}^T (\Delta \mathbf{r}_{j/k} - \epsilon \Delta^{\mathcal{B}_k} \mathbf{v}_{j/k}), \quad (3.32)$$

where  $\Delta \mathbf{r}_{j/k}$  is the position error and  $\Delta^{\mathcal{B}_k} \mathbf{v}_{j/k}$  is the velocity error. In the context of the problem, it is assumed that the exact position is known, but it is still estimated. Therefore, we assume  $\Delta \mathbf{r}_{j/k}$  is negligible. This simplification allows the function of gains to be pulled outside of the double summation and used to scale this term in the Lyapunov derivative. Under this simplification,  $\dot{V} \leq 0$  when

$$\mathbf{z}^T D \mathbf{z} > \epsilon \sum_{k=1}^N \sum_{j=1}^N \|\mathcal{B}_k \mathbf{a}_{j/k}^T \Delta^{\mathcal{B}_k} \mathbf{v}_{j/k}\|. \quad (3.33)$$

Hence, solutions that lie outside the bound  $\mathbf{z}^T D \mathbf{z} = \epsilon \sum_{k=1}^N \sum_{j=1}^N \|\mathcal{B}_k \mathbf{a}_{j/k}^T \Delta^{\mathcal{B}_k} \mathbf{v}_{j/k}\|$ , will approach this boundary. Once inside, solutions will remain there because  $\dot{V} < 0$  in the region outside the boundary.  $\square$

We can choose  $K_1$  and  $K_2$  so that  $\epsilon$  is small, allowing the vehicles to approach arbitrarily close to the circular formation. Simulation results displayed in Fig. 3.4 illustrate the observer-based feedback control algorithm converging to a circular formation. Note that the error in the estimates approaches zero in steady-state,

which implies that each vehicle determines the relative position and relative velocity of the other vehicles as time goes to infinity.

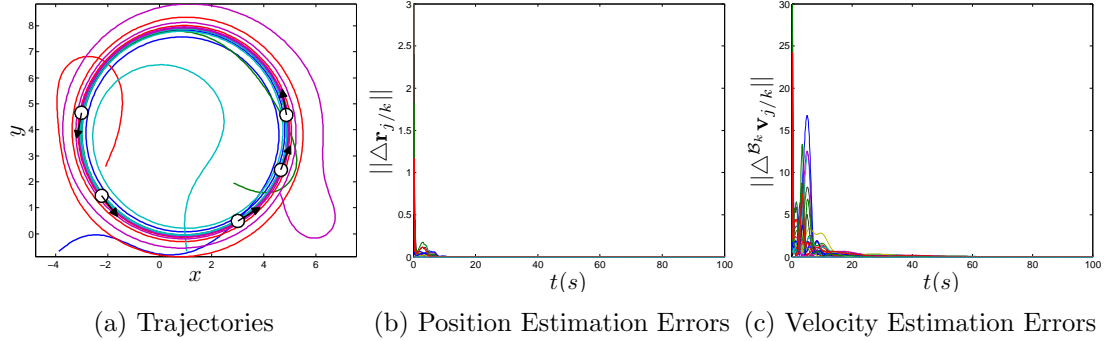


Figure 3.4: A simulation of five self-propelled vehicles performing the circular control law using the observer-based feedback control algorithm with  $\omega_0 = 0.25$ . Each vehicle is given a random initial position and velocity;  $K = 1$ ,  $K_p = 1$ ,  $K_1 = 10$ , and  $K_2 = 100$ .

With theoretical justification behind the observer-based feedback control algorithm, the next step is to perform the derived control laws on a more realistic system for validation. Before implementation on a miniature submarine platform described in Chapter 5, a six degree of freedom model was constructed to mimic the vehicle's behavior. The cooperative control laws are then applied to this higher fidelity model for analysis.

## Chapter 4

### Simulation Results

The vehicle model used above is useful in developing control laws, but does not take into account the dynamics of a physical system performing that control. Therefore, we have developed a higher fidelity model of our miniature submarine that comprises our laboratory scale testbed. Simulation of this model provides a prediction of the vehicle's behavior before experimental testing is performed.

#### 4.1 Six Degree of Freedom Submarine Model

This higher fidelity model is derived using an inertial frame and body frame. The inertial frame,  $\mathcal{I} = (O, \mathbf{g}_x, \mathbf{g}_y, \mathbf{g}_z)$ , is affixed to the ground at point  $O$  with the positive  $\mathbf{g}_z$  direction into the ground. The  $\mathbf{g}_x$  and  $\mathbf{g}_y$  directions can be arbitrarily chosen, but must be constrained such that  $\mathbf{g}_x \times \mathbf{g}_y = \mathbf{g}_z$ , to maintain a right-handed coordinate system. The body fixed frame,  $\mathcal{B} = (P, \mathbf{b}_1, \mathbf{b}_2, \mathbf{b}_3)$  is attached to the body of the submarine at point  $P$  which coincides with the vehicle's center of mass. The principle axes of this frame are chosen according to aircraft convention such that  $\mathbf{b}_1$  is out the nose of the vehicle,  $\mathbf{b}_2$  is out the right side, and  $\mathbf{b}_3$  is out the belly of the submarine.

With these frames defined, the forces on the body displayed in Fig. 4.1 can

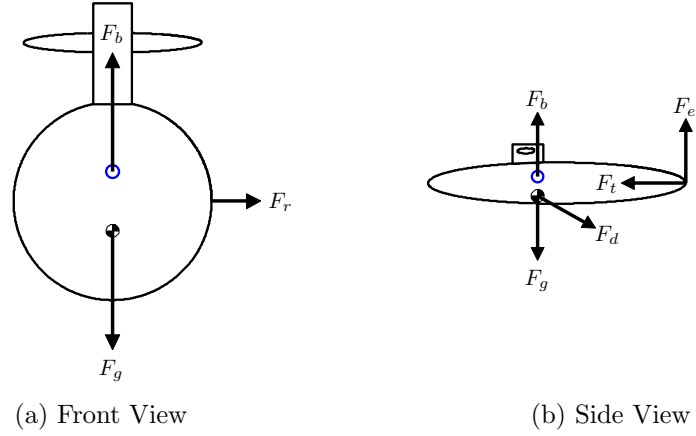


Figure 4.1: Free-body diagram of submarine model

Submarine Properties						
Mass(kg)	Length(m)	Width(m)	Height(m)	$I_1$ (kg/m <sup>2</sup> )	$I_2$ (kg/m <sup>2</sup> )	$I_3$ (kg/m <sup>2</sup> )
7.79	0.991	0.165	0.165	0.212	0.393	0.393
$S_1$ (m <sup>2</sup> )	$S_2$ (m <sup>2</sup> )	$S_3$ (m <sup>2</sup> )	$S_e$ (m <sup>2</sup> )	$S_r$ (m <sup>2</sup> )		
.0214	.128	.128	.0016	.0019		

Table 4.1: Physical miniature submarine properties

be defined as

$$\begin{aligned}
 F_g &= mg\mathbf{g}_z \\
 F_b &= -\rho_w V g\mathbf{g}_z \\
 F_t &= 35u_t\mathbf{b}_1 \\
 F_d &= -q_{\infty_1}S_1C_d\mathbf{b}_1 - q_{\infty_2}S_2C_d\mathbf{b}_2 - q_{\infty_3}S_3C_d\mathbf{b}_3 \\
 F_r &= 2q_{\infty_1}S_r \sin(u_r\pi/4)\mathbf{b}_2 \\
 F_e &= 2q_{\infty_1}S_e \sin(u_e\pi/4)\mathbf{b}_3
 \end{aligned} \tag{4.1}$$

where  $F$  represents a force,  $u$  represents control input from -1 to 1,  $C_d$  is the drag coefficient,  $m$  represents the vehicle's mass,  $\rho_w$  is the density of water,  $V$  is the volume of displaced water, and  $q_{\infty}$  refers to the instantaneous dynamic pressure

along a particular direction of the body frame denoted by the subscript number. The subscripts on the force and control terms refer to a specific force or input. In this model, the subscript  $g$  refers to gravity,  $b$  to buoyancy,  $t$  to thrust,  $d$  to drag,  $r$  to rudder, and  $e$  to the dive planes. The other terms in (4.1) relate to physical properties of the vehicle and are defined in Table 4.1.

## 4.2 Numerical Integration of Submarine Model

The forces described above determine how the submarine model will translate and rotate in time. More specifically, the translational and rotational equations of motion for the submarine model obey Euler's equations and are defined according to aircraft convention with a 3-2-1 Euler angle rotation sequence [14]. Integration of the twelve equations of motion produce the submarine's position, velocity, body rates, and Euler angles in time which are used to evaluate the vehicle's performance.

The actual integration of these equations of motion was performed using a first-order Euler integration scheme shown in (4.2) where  $t$  represents a specific time and  $\Delta t$  represents the time step. The subscripted  $F$ 's and  $M$ 's refer to forces and moments along the subscript's frame direction, respectively. Although this integration method may not be as accurate as other schemes, it allows for real-time application of control signals at discrete intervals. These signals are provided autonomously or via a user interface in real-time. This discrete application of control is used to mimic our underwater-vehicle testbed control structure which runs at two separate frequencies. Control to the submarine's dive planes is provided at 20 Hz,

which is matched by the simulator exactly. The onboard rudder control runs at 50Hz, which is simulated at a slightly faster frequency of 60Hz. In addition to the discrete control application, a visual framework is also used to provide the user with continuous feedback.

$$\begin{aligned}
x(t + \Delta t) &= x(t) + \dot{x}\Delta t \\
y(t + \Delta t) &= y(t) + \dot{y}\Delta t \\
z(t + \Delta t) &= z(t) + \dot{z}\Delta t \\
\dot{x}(t + \Delta t) &= \dot{x}(t) + (\sum F_x/m)\Delta t \\
\dot{y}(t + \Delta t) &= \dot{y}(t) + (\sum F_y/m)\Delta t \\
\dot{z}(t + \Delta t) &= \dot{z}(t) + (\sum F_z/m)\Delta t \\
\phi(t + \Delta t) &= \phi(t) + (w_1 + \omega_2 \sin \phi \tan \theta + \omega_3 \cos \phi \tan \theta)\Delta t \\
\theta(t + \Delta t) &= \theta(t) + (\omega_2 \cos \phi - \omega_3 \sin \phi)\Delta t \\
\psi(t + \Delta t) &= \psi(t) + (\omega_2 \sin \phi + \omega_3 \cos \phi) \sec \theta \Delta t \\
\omega_1(t + \Delta t) &= \omega_1(t) + \frac{\sum M_1 - (I_3 - I_2)w_2w_3}{I_1} \Delta t \\
\omega_2(t + \Delta t) &= \omega_2(t) + \frac{\sum M_2 - (I_1 - I_3)w_1w_3}{I_2} \Delta t \\
\omega_3(t + \Delta t) &= \omega_3(t) + \frac{\sum M_3 - (I_2 - I_1)w_1w_2}{I_3} \Delta t
\end{aligned} \tag{4.2}$$

These equations of motion define the submarine's movement in a three-dimensional world. Collective behaviors such as spirals and circular formations on the surface of a sphere [5] exist in this higher degree of freedom world. However, the cooperative control algorithms in this paper have been designed for a planar case. Therefore, the submarine model will need to implement a depth controller to constrain a translational degree of freedom. Once depth is stabilized, the cooperative control algorithm

resembles the planar case with the submarine's yaw angle equivalent to the planar velocity orientation.

Stabilization of depth is achieved using a proportional-integral controller on the error between the vehicle's actual and desired depth. A simple proportional controller will not be effective in this case, because an offset in the dive planes is required to provide a counteracting force opposing the buoyancy force. The integral term determines the required offset and stabilizes the system with respect to depth.

### 4.3 Simulated Cooperative Control Algorithms

The simulation architecture for the submarine model runs on an object-oriented programming language, which allows the submarine model to be replicated to  $N$  identical vehicles used to test the cooperative control laws. We begin by testing the parallel and circular control laws without estimation defined in (2.2) and (2.4). Validation of these control laws is essential before testing the more complex observer-based feedback control algorithm, which is built upon its predecessor. In addition to having the formation converge, we are also interested in seeing that the other states of the model remain stable.

#### 4.3.1 Parallel & Circular Control

In order to perform the cooperative control laws defined in Chapter 2, some modifications to these laws are necessary. For the parallel control law, the vehicle model assumes that the relative velocity orientation between vehicles is known.

Our physical testbed cannot directly measure the velocity of the submarines, but it can tell us the position and pose of the vehicle. With this knowledge, we assume that the submarine’s velocity aligns with the orientation of the body. Although this assumption is generally not true, vehicles traveling in a straight line will not exhibit any sideslip angle. Therefore, submarines in a parallel formation should each maintain a zero sideslip angle as well. Under this assumption, the control law in (2.6) becomes

$$u_k = K_p(\alpha_k(\boldsymbol{\psi}) - \omega_k), \quad (4.3)$$

where  $\boldsymbol{\psi}_k = [\psi_1 - \psi_k, \dots, \psi_N - \psi_k]^T$ .

Note that the yaw angles  $\psi_k$ , are used to determine the relative velocity orientation. The yaw angles are used because they are equivalent to velocity orientation in the planar case when depth is managed. A five vehicle simulation of this control law is shown from an overhead view in Fig. 4.2. Note that just like the particle model, each submarine is able to converge to the desired formation with little oscillation about the final direction.

This simulation displays that the submarine models are able to manage depth as well as perform the collective behavior. In addition to achieving this goal, each vehicle’s body rates and velocities reach a constant value as  $t \rightarrow \infty$ . These constant values imply that each vehicle reaches a stable steady-state behavior and will remain there.

Similar to the parallel control law, the circular control law requires some slight modifications before implementation. The assumption that the submarine’s yaw

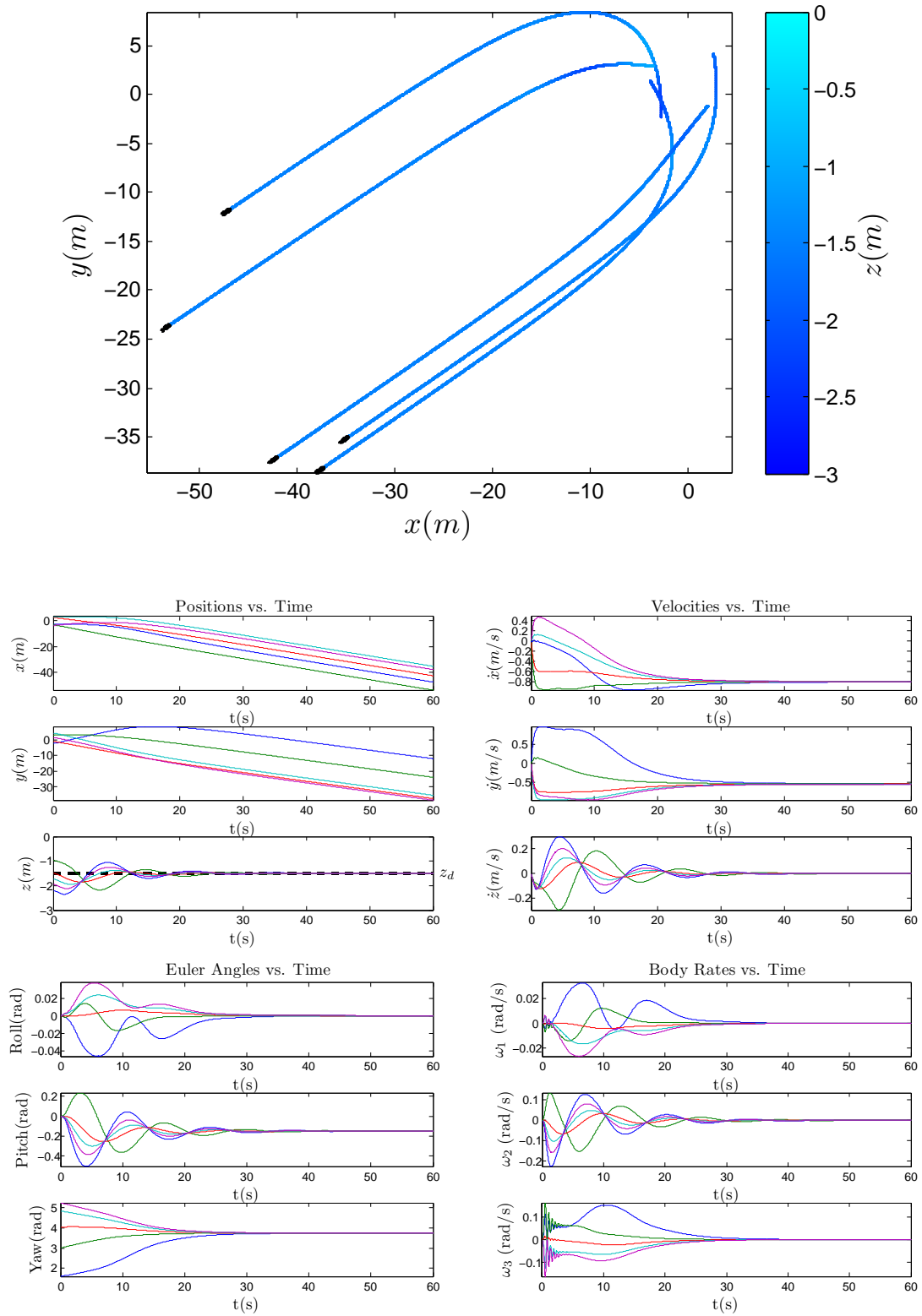


Figure 4.2: A simulation of five submarine models performing the parallel control law;  $K = -1$  and  $K_p = 1$ .

angle is equivalent to its velocity heading when depth is constant, no longer holds in this case. Instead, when a submarine is traveling in a circle, a constant sideslip angle is reached [13] causing a discrepancy between the vehicle orientation and velocity orientation. If the vehicle's orientation is utilized, the center of rotation calculation (2.3) will be incorrect.

However, if we know the submarine's sideslip angle  $\beta_k$ , this center of rotation calculation could be corrected. For the identical submarine models used in the simulator, each submarine's sideslip angle will be identical to the others and related to the desired circle size. On our physical miniature submarine platform, this value will vary from platform to platform. Therefore, our modified control law will need to be robust to platform variance. As mentioned earlier, our testbed cannot directly sense the velocity of the vehicle, but we can estimate this quantity using the position in time. For simulation purposes, the vehicle's velocity is directly used resulting in the following circular control law

$$\nu_k = \omega_0(s_k + K\mathcal{P}_k\mathbf{c}[\cos(\psi_k - \beta_k) \quad \sin(\psi_k - \beta_k)]^T) \quad (4.4)$$

where  $\mathbf{c} = [\mathbf{c}_1, \dots, \mathbf{c}_N]^T$ ,  $s_k$  is submarine  $k$ 's speed,  $\beta_k$  is the sideslip angle, and  $\mathbf{c}_k = [\mathbf{r}_k]_X + \omega_0^{-1}[-\sin(\psi_k - \beta_k) \quad \cos(\psi_k - \beta_k)]_X^T$ . This modification produces circular motion with an approximate radius of  $|\omega_0|^{-1}$ . A five vehicle simulation of this implementation is displayed from an overhead view in Fig. 4.3. Note that each vehicle's turning rate converges to  $s_k\omega_0$ .

This simulation also shows that the submarine models are able to manage

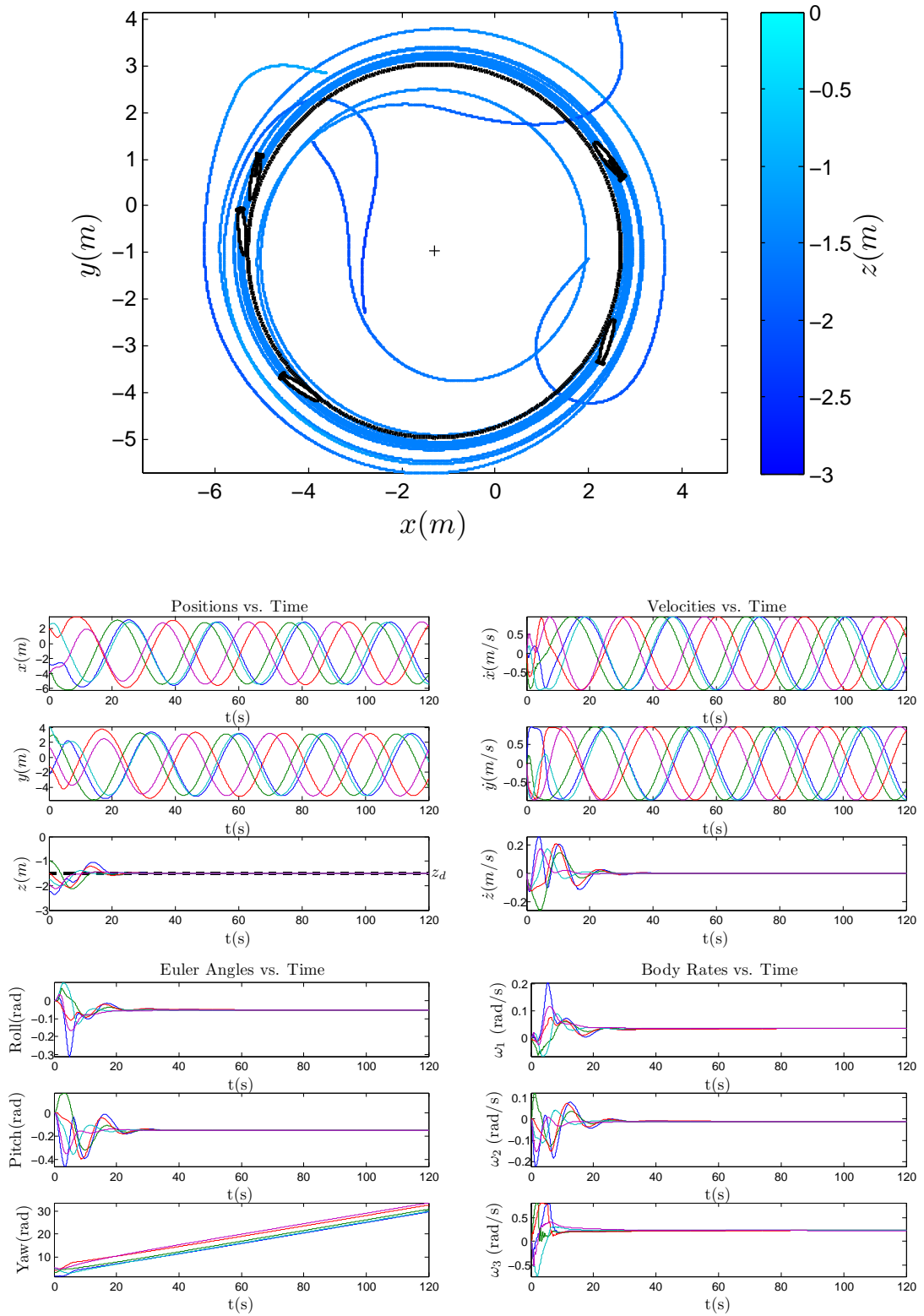


Figure 4.3: A simulation of five submarine models performing the circular control law;  $K = 1$  and  $K_p = 1$ .

depth as well as perform circular trajectories. In addition to collective motion, each submarine’s steady-state behavior suggests that the platform is stable. With validation that both parallel and circular control laws are stable onboard the higher fidelity model, simulation of the observer-based feedback control algorithm can be performed.

### 4.3.2 Observer-Based Feedback Control

In order to perform the observer-based feedback control algorithm, every submarine needs to maintain estimates for every other model in their own path frame. This estimation is achieved by integrating (3.9) with a first-order Euler integration scheme with respect to the vehicle’s path frame that is aligned with the submarine’s velocity. With these estimates defined, the relative velocity orientation is computed, followed by the control algorithms described above. Note that both collective algorithms no longer require that each vehicle has knowledge of every other vehicle’s velocity orientation or sideslip angle because the estimates provide that information. However, implementation of the control algorithm onboard a vehicle still requires knowledge of that vehicle’s own velocity orientation or sideslip angle.

Simulations of this control onboard the submarine model have often displayed an oscillatory behavior around the desired trajectory with identical control gains used on the vehicle model. These oscillatory motions are illustrated in Fig. 4.4. When examining the errors in the estimated position and velocity, we notice that they do not converge to zero, but rather, are bounded according to Lemma 3.

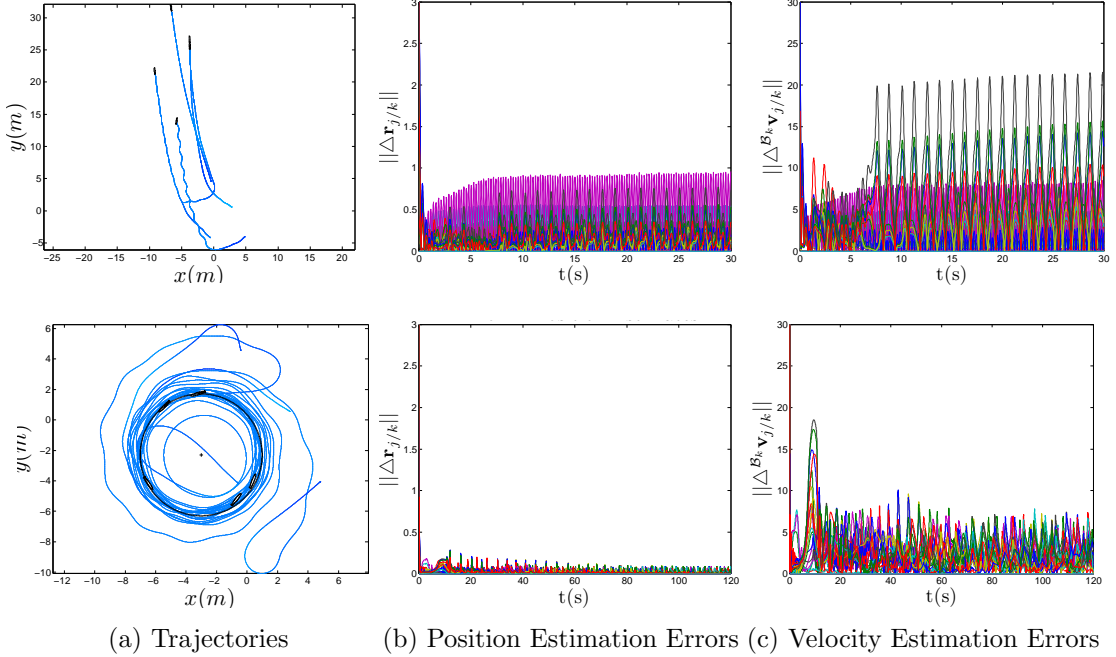


Figure 4.4: Simulations of five submarine models performing the observer-based feedback control algorithm in which they exhibit oscillatory behavior;  $K_1 = 10$  and  $K_2 = 100$ .

Understanding that the oscillation is a result of the perturbation term in the estimator dynamics, gives us some options as to how to further reduce the impact of this term. Based on theory, reducing  $\epsilon$  should allow the formation to come arbitrarily close to the particular formations as discussed in Theorems 4 and 5. Small reductions in  $\epsilon$  require that the choice of  $K_2$  increase dramatically. This gain choice is not a valid option for our Euler integration scheme, which has a greater probability of approaching instability the higher  $K_2$  becomes.

Therefore, instead of altering the estimator gains,  $K$  can be chosen to slow down the convergence of the system. In addition to slowing down the formation,  $K$  will decrease the vehicle's turning rate, and ultimately reduce the time varying perturbation  $\mathbf{g}_{j/k}(t)$ , in which the turning rate is embedded.

For a parallel formation, simply reducing  $K$  is not sufficient because the perturbation also increases proportional to the distance between vehicles. This relationship makes sense intuitively because slight variations in velocity orientation would be harder to extract from larger distances. For example, imagine sitting on a beach and watching a cargo ship in the distance. Determining its exact velocity orientation by watching it move, is not a trivial calculation. Our problem goes one step further in which the observer is not stationary, but is free to translate and rotate. Taking this point into consideration, a scheduled gain choice of  $K = 9.99\|\hat{p}_\theta\| - 10$  was implemented onboard the model where  $\hat{p}_\theta$  represents the alignment of the system using velocity orientation estimates. When the vehicles are in a balanced formation,  $\|\hat{p}_\theta\| = 0$ , creating a large  $K$  gain. This large gain causes the submarines to converge quickly. When the collective is in a parallel formation,  $\|\hat{p}_\theta\| = 1$ , creating a small  $K$  gain. This gain choice reduces the speed of convergence as well as the rotational movement of the model. The reduction allows the estimates to converge, and ultimately, the formation converges as well, as indicated in Fig. 4.5.

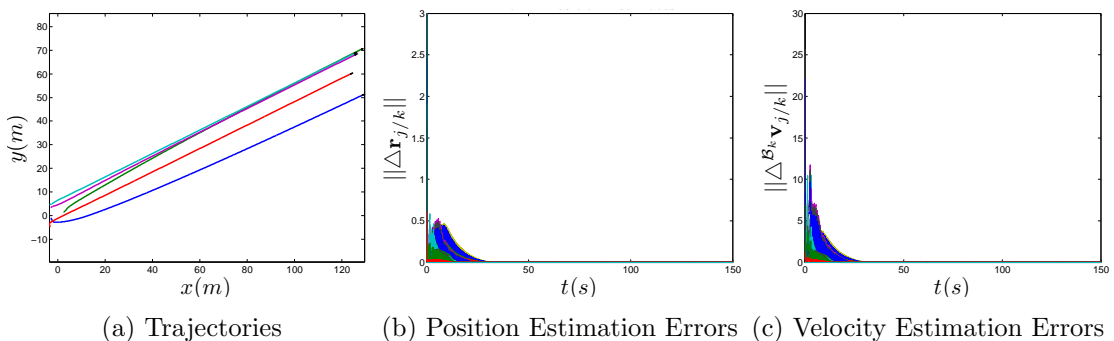


Figure 4.5: A simulation of five submarine models performing the scheduled parallel control law;  $K = 9.99\|\hat{p}_\theta\| - 10$ ,  $K_p = 1$ ,  $K_1 = 10$ , and  $K_2 = 100$ .

For circular motion, reducing  $K$  alone allows the formation to approach the

circular formation as displayed in Fig. 4.6. Although there is still slight error in the estimates, the general circular pattern of the formation is reproduced. Controllers with scheduled gains have also been implemented on this model, altering the gain  $K$  as a function of how close the vehicles' centers of rotation are aligned. These simulations produced very similar results as those shown in Fig 4.6.

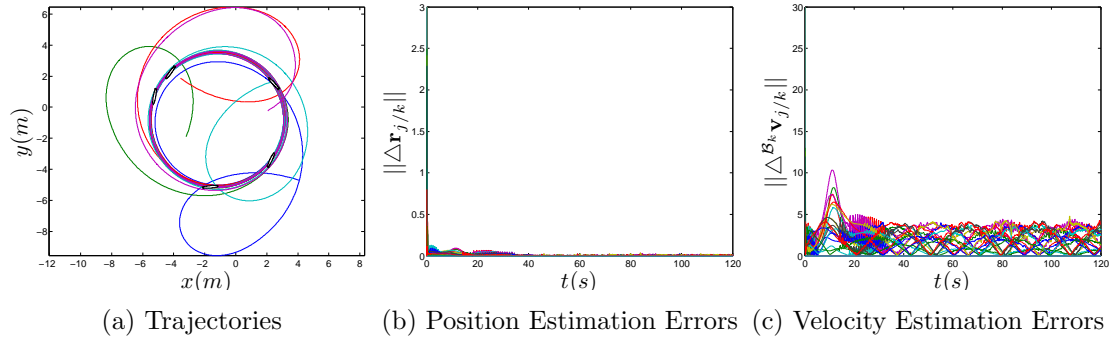


Figure 4.6: A simulation of five submarine models performing the circular control law with small alignment gain and  $\omega_0 = 0.25$ ;  $K = .1$   $K_p = 1$ ,  $K_1 = 10$ , and  $K_2 = 100$ .

## Chapter 5

### Experimental Results

As previously mentioned, the proposed control laws have been designed for an idealized model that does not take into account the individual dynamics of a physical platform. Validation of these control algorithms is achieved through the implementation of closed-loop control onboard a testbed of miniature submarines. More specifically, each submarine's trajectory is recorded and compared against the formation that should emerge. Submarine trajectories that coincide with the vehicle model validate that the control law is a viable option for similar platforms.

#### 5.1 Underwater-Vehicle Testbed

The submarines used in the testbed are 1:60 scale models of the U.S.S. Albacore which have been modified to operate via remote control as shown in Fig. 5.1. Inside each vehicle's hull are two separate pressure vessels. The smaller vessel at the nose of the craft is used as the battery compartment. Behind that enclosure lies the main pressure vessel which houses the electronics as displayed in Fig 5.2. The vessels have an insulated wire connection between them providing power to the electronics. The two-pressure vessel design allows the main pressure vessel's water-tight seal to remain intact, while swapping out used batteries for new ones.

Although the submarine is a replica of the U.S.S. Albacore, the model does

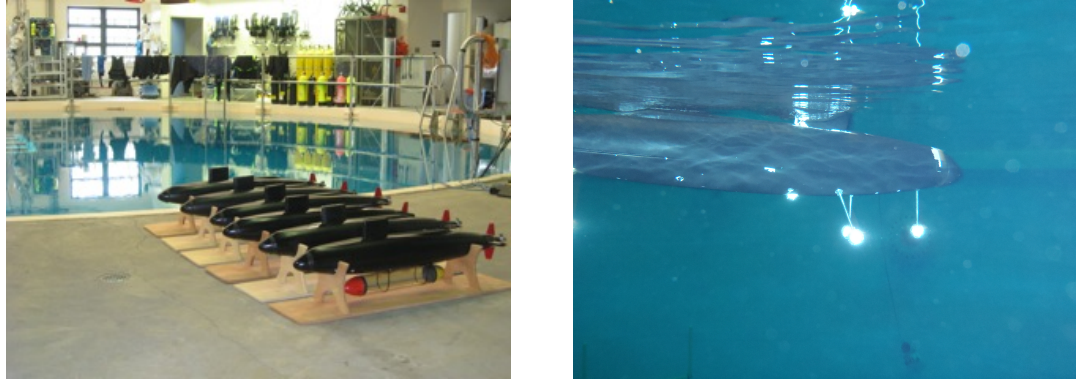


Figure 5.1: Miniature submarine models of the U.S.S. Albacore that comprise the underwater vehicle testbed

not utilize a ballast system to regulate depth. Instead, the submarine is described as a dynamic diver because it uses its velocity and dive planes to remain underwater. Under this classification, the vehicle is weighted close to neutral buoyancy, but slightly positive. This choice in buoyancy allows the dive planes to be more effective since they have to counteract a small rising force. In addition, the weighting of the submarine allows for surfacing by simply turning off the propeller in emergencies.

Communication to the vehicle is provided by a 72Mhz radio transmitter and receiver. The transmitter and corresponding receiver utilize a matching crystal that allows control signals to be passed from the transmitter to the receiver. The crystals are manufactured in several channels, which allow multiple vehicles to function at the same time without interference. In application, the wireless communication functions to a depth of approximately 3 meters. Once that depth is surpassed, the signal attenuates and the connection is broken. This signal loss initializes the motor's failsafe mechanism, stopping the propeller. The submarine then rises back into communication range where control is resumed.

In its current configuration, the submarine is designed to operate under human

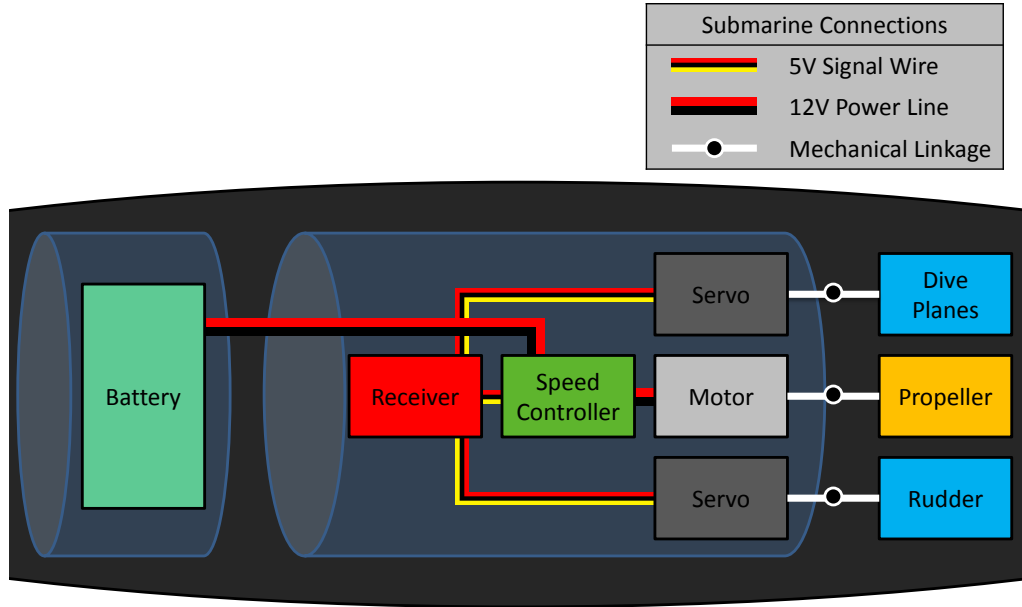


Figure 5.2: Wiring diagram for remote operation

control. Altering the vehicle’s setup to an autonomous configuration is achieved in two stages. The first stage is accomplished by adding a microcontroller onboard each vehicle. More specifically, an arduIMU+ board [1] is affixed inside the main pressure vessel. This board contains three accelerometers and three gyroscopes aligned along three orthogonal axes. In addition to its sensing capability, a programmable ATMEGA328 chip is used to poll these sensors inside of a customizable control loop.

In our submarine, this board is placed between the receiver and servo, which controls the rudder as illustrated in Fig. 5.3. The receiver provides the board with power and a pulse width modulation signal. In standard operation, the servo interprets this signal and rotates to a prescribed angle defined by the width of the pulse. In the autonomous configuration, the pulse width is read by the microcontroller and is linearly mapped to a desired yaw rate. This rate is used in a proportional state feedback controller with the yaw rate gyroscope. The resulting control signal

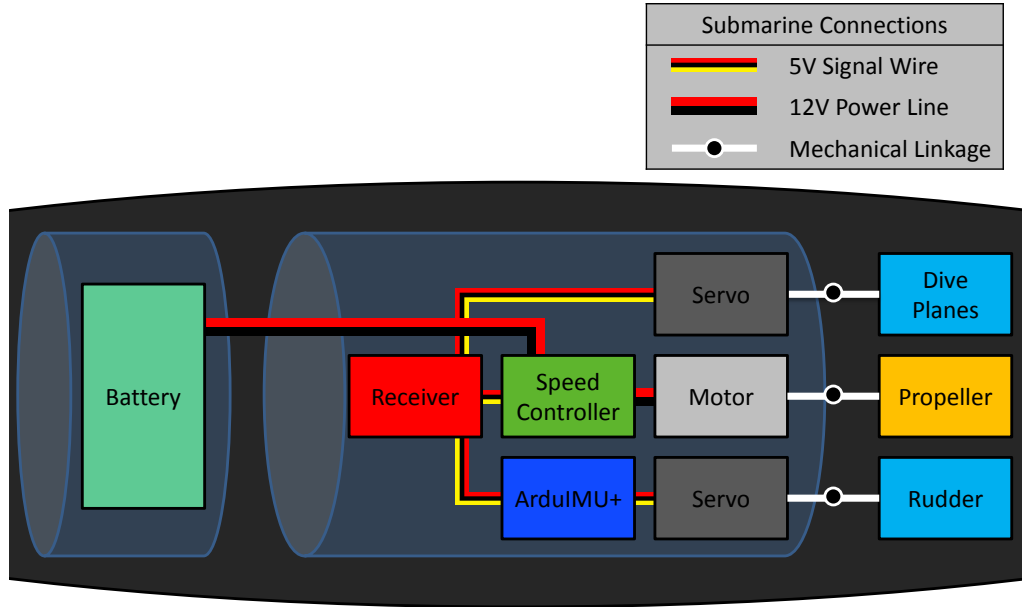


Figure 5.3: Wiring diagram for autonomous operation

from this calculation is linearly mapped back to a pulse width. This new signal is then passed to the servo and rotates the rudder. Pseudocode for this control implementation is shown in Fig. 5.4.

The addition of the microcontroller to the submarine alters the functionality of the rudder control stick on the transmitter. Rather than controlling the deflection of the rudder, the user now controls a desired turning rate for the vehicle. The arduIMU+ board closes the loop and stabilizes the yaw rate within the physical limitations of the vehicle. With the submarine's yaw rate stabilized by control, the second stage to autonomous operation removes the user from the control loop via the transmitter's trainer port. The trainer port is typically used to teach another individual how to operate the vehicle. In this case, the trainer gives control of the submarine to a trainee's transmitter by engaging a switch located on his own transmitter. When disengaging the switch, the trainer takes back control of the

```

begin
  Initialize a pin for reading the width of a pulse
  Initialize a pin for writing pulse width modulation
  Initialize a current desired yaw rate variable to zero
  Initialize a previous desired yaw rate variable to zero
  Initialize the actual yaw rate variable to zero
  while operating
    if a pulse is detected
      Read incoming pulse width
      Set current desired yaw rate to the linear mapping result from pulse width to yaw rate
    else the submarine is out of transmission range
      Set the current desired yaw rate to the previous desired yaw rate
    end
    Set the actual yaw rate to the gyroscope reading
    Compute control value from the current desired yaw rate and actual yaw rate
    Convert control value to a pulse width
    Send pulse to servo
    Set the previous desired yaw rate to the current desired yaw rate
  end
end

```

Figure 5.4: Pseudocode running onboard the arduIMU+ board

submarine. The autonomous configuration replaces the trainee and his transmitter with a computer through a PCTx interface [18].

The PCTx interface allows a computer to command the control sticks of a transmitter. In addition, a single computer may operate multiple transmitters simultaneously by adding additional interfaces. This functionality allows for autonomous operation of multiple vehicles, and is one of our key goals. Computing the desired control laws to steer each vehicle requires knowledge of the submarines' states. These properties are obtained by a Qualisys Motion Capture System [19] described next.

## 5.2 Qualisys Motion Capture System

The Qualisys Motion Capture System utilizes twelve underwater cameras to track the position of retroreflective markers. Six markers are affixed to the hull of each submarine in different, varying configurations. The motion capture system defines rigid bodies based on the placement of the markers with respect to their counterparts. The varying configurations are required so that the system can track multiple vehicles. As long as three markers are tracked by the system, the submarine's position and pose can be calculated. It is important to note that the placement of markers with similar or symmetric patterns will confuse the system's interpretation of the rigid bodies, resulting in poor tracking.

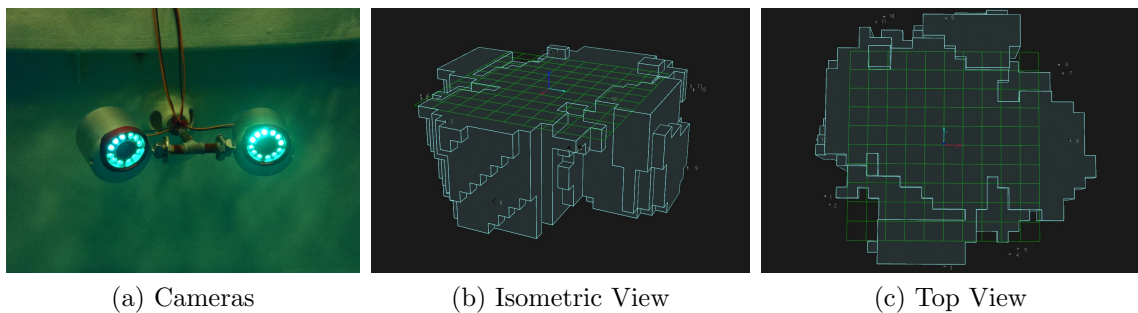


Figure 5.5: Qualisys Motion Capture System

With well-defined placement of markers for our submarine models, tracking their position and pose can be achieved in real-time with the provided source code. In addition to polling this data at 20Hz, the system can also record the vehicle's motion for postprocessing. As mentioned in Chapter 4, the system can only provide the vehicle's position and pose. However, some control implementations require knowledge of the vehicle's velocity direction and turning rate. These values

are determined via a differencing approach between measurements. Although the estimation method is influenced by tracking losses, the estimates are required to compute the desired control.

With measurements available to perform the control laws, the automation loop can be closed by combining the Qualisys and PCTx source codes. The autonomous control loop starts by retrieving the states of each vehicle being tracked. The control laws use these states to determine an elevator deflection and desired turning rate for each vehicle based on the control laws. These control signals are then passed down to the submarines through the PCTx interface, closing the loop. Fig. 5.6 displays the control architecture discussed above.

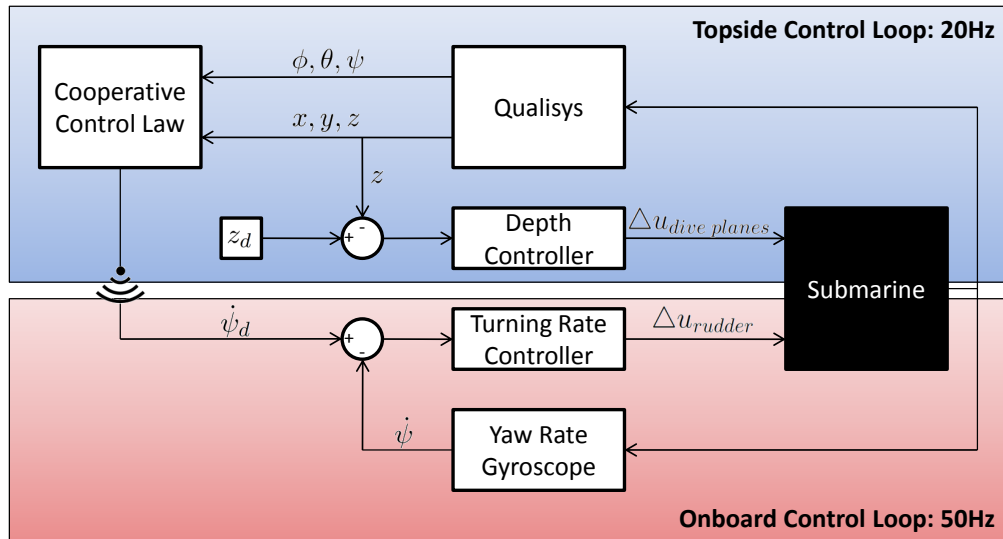


Figure 5.6: Control architecture for the underwater vehicle testbed.

### 5.3 Experimental Results of the Underwater Vehicle Testbed

The autonomous vehicle design discussed above was installed in the Neutral Buoyancy Research Facility at the University of Maryland, College Park. The testbed operates within the tank, which is 25 feet deep and 50 feet across, and is also equipped with twelve Qualisys underwater cameras. Camera placement is crucial for maximizing the capture volume which is shown in Fig. 5.5.

With this control architecture in place, validation of the cooperative control laws can be achieved. To begin testing, a single submarine combined with a virtual vehicle in the tank is used. The virtual vehicle is unaware of the submarine in the tank and holds its current parallel or circular formation. The submarine is able to "see" the virtual vehicle and computes the desired control with the virtual vehicle, being part of its group. This distinction allows the virtual vehicle to steer the submarine to a preset formation, because its control is independent of the other vehicles in the group [22].

#### 5.3.1 Virtual Vehicle Experiments

In parallel experiments, the virtual vehicle travels along the positive  $x$  axis of the tank. In theory, the submarine should minimize the relative orientation angle between the virtual vehicle and itself, resulting in both vehicles traveling along the same direction. Fig. 5.7 shows three experimental tests of this particular formation. Note that in each experimental run, the submarine begins with a large error in relative orientation angle; but, by the time it reaches the edge of the tank, the

difference is minimal. Although theory and simulation demonstrate that the relative orientation between vehicles goes to zero, we do anticipate slight oscillations about this point due to sensor noise in the system. Based on these test runs, parallel control with a virtual vehicle is validated because phase synchronization was achieved by the submarine, repeatedly.

With the parallel formation validated, we continue the virtual vehicle experiments with the circular formation. The circular control law was implemented with a virtual vehicle circling the center of the tank with a radius of 2.5 meters. In this case, we accounted for the submarine's velocity heading not being aligned with the orientation of the rigid body by the estimation discussed earlier. In the experimental test runs, the submarine starts around the virtual vehicle's circular trajectory and begins to encircle the center of the tank as shown in Fig. 5.8. The radius of the circle traced out by the submarine does not match the radius of the virtual vehicle exactly; however, the submarine does stabilize to a constant offset of approximately 0.1 meters. The error in the centers of rotation is attributed to the measurement noise being neglected in our calculations. Similar to the parallel formation, these experimental tests validate that the circular formation is feasible for implementation on a physical platform.

### 5.3.2 Multi-Vehicle Experiments

With validation of a single submarine's capability to perform the desired motion completed, multi-vehicle experiments were then conducted. For this configura-

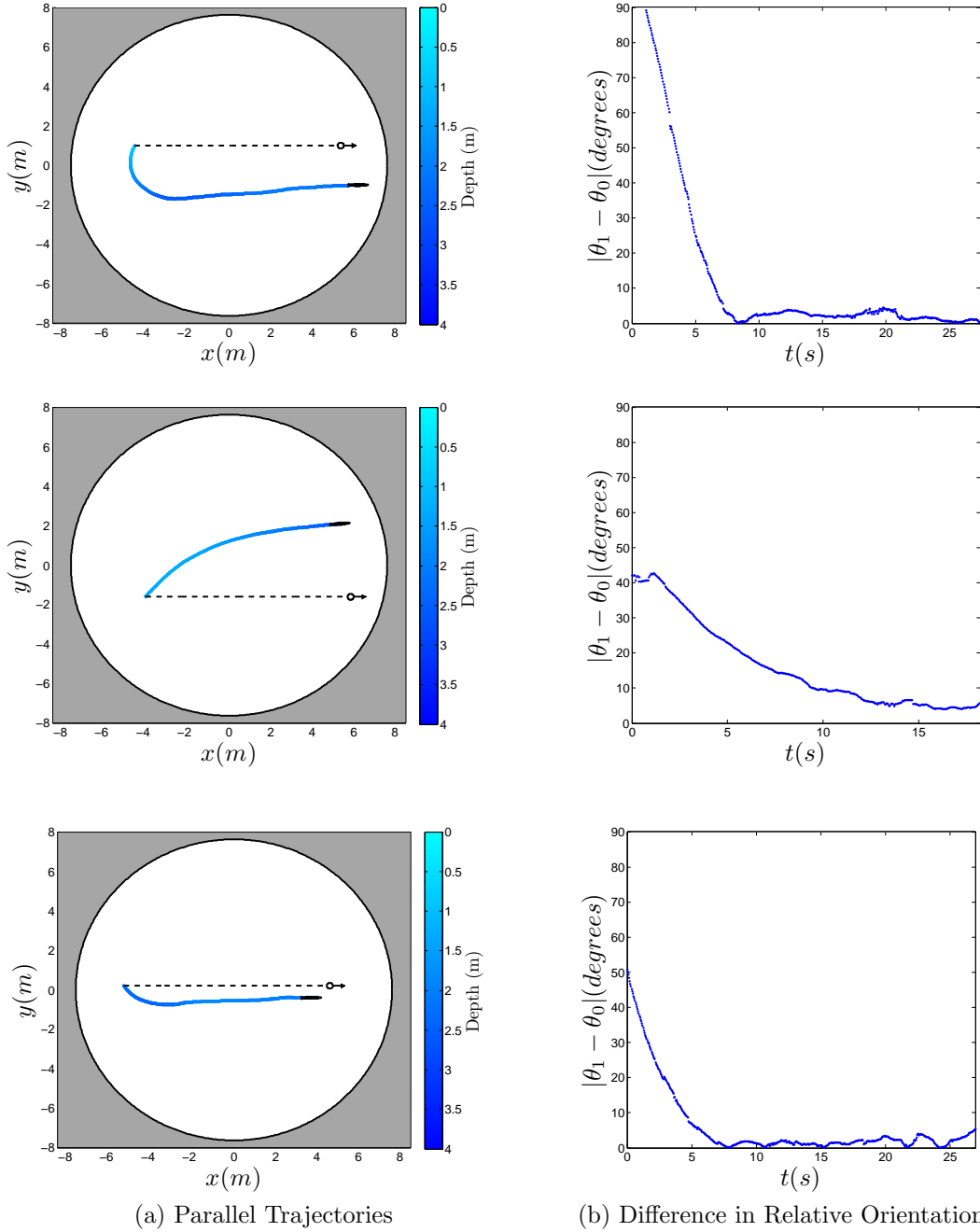


Figure 5.7: Experimental test runs of a single submarine performing the parallel control law with a virtual vehicle.

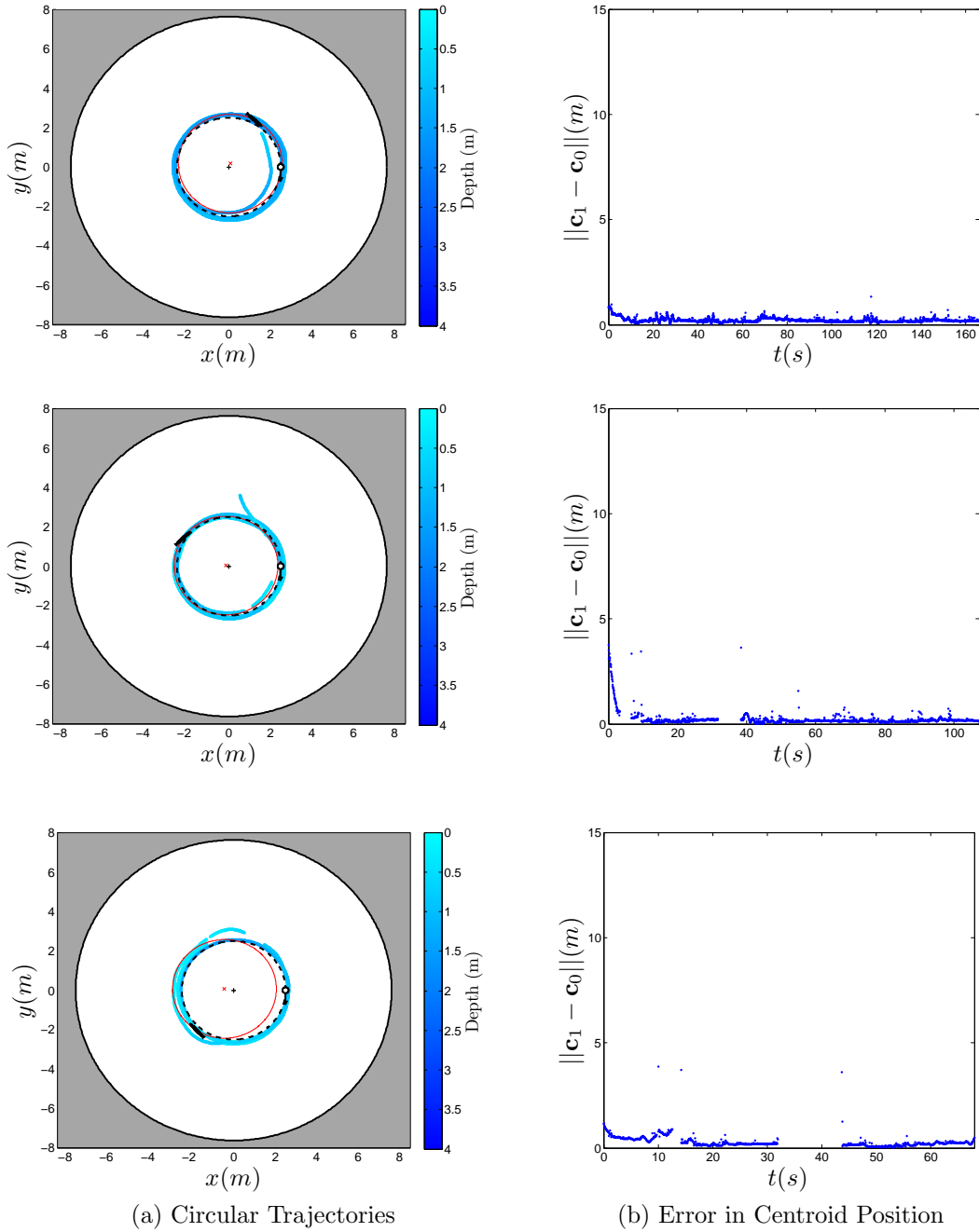


Figure 5.8: Experimental test runs of a single submarine performing the circular control law with a virtual vehicle.

tion, we remove the virtual vehicle, allowing the submarines to collectively decide their overall formation. The resulting formation is determined by the initial conditions and vehicle dynamics. Utilizing the vehicle and submarine model, final vehicle trajectories can be predicted given their initial conditions. Using this knowledge, the initial conditions of the submarines were contrived to optimize the use of the tank.

For the parallel formation, two submarines were started within close proximity to each other with orientation differences ranging from 30 to 55 degrees as shown in Fig. 5.9. Two submarines will minimize this difference by rotating toward each other until they have reached a parallel formation. The three experimental tests performed, indicate that the control law is operating as we would expect, but with larger errors than those seen by the the virtual vehicle experiments. This decline in performance is anticipated, because the virtual vehicle experiments had complete control of one vehicle, not corrupted by sensor noise. Adding the second submarine creates additional noise as well as the complexity of another vehicle's dynamics to the problem. However, even with the vehicle addition, the parallel behavior still emerges.

In similar fashion, the circular control was also tested with two submarines as shown in Fig. 5.10. Initial conditions were contrived using the vehicle and submarine models to have the final trajectories remain around the center of the tank. In these tests, the submarines are trying to stabilize around the same circle with a 3 meter radius. In comparison to the virtual vehicle experiments, these tests, in general, fair worse. However, the results do show promising behavior in that the vehicles

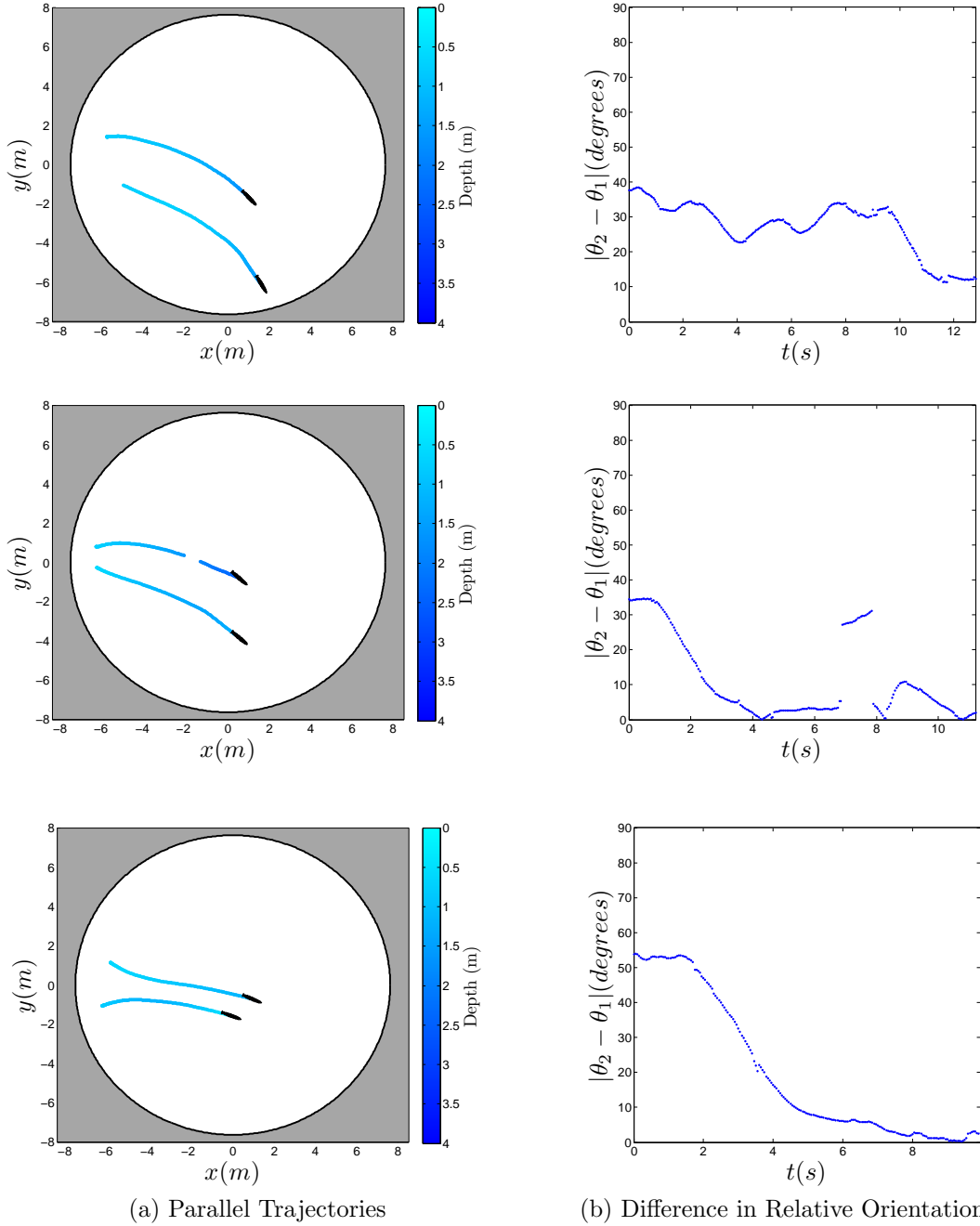


Figure 5.9: Experimental test runs of two submarines performing the parallel control law.

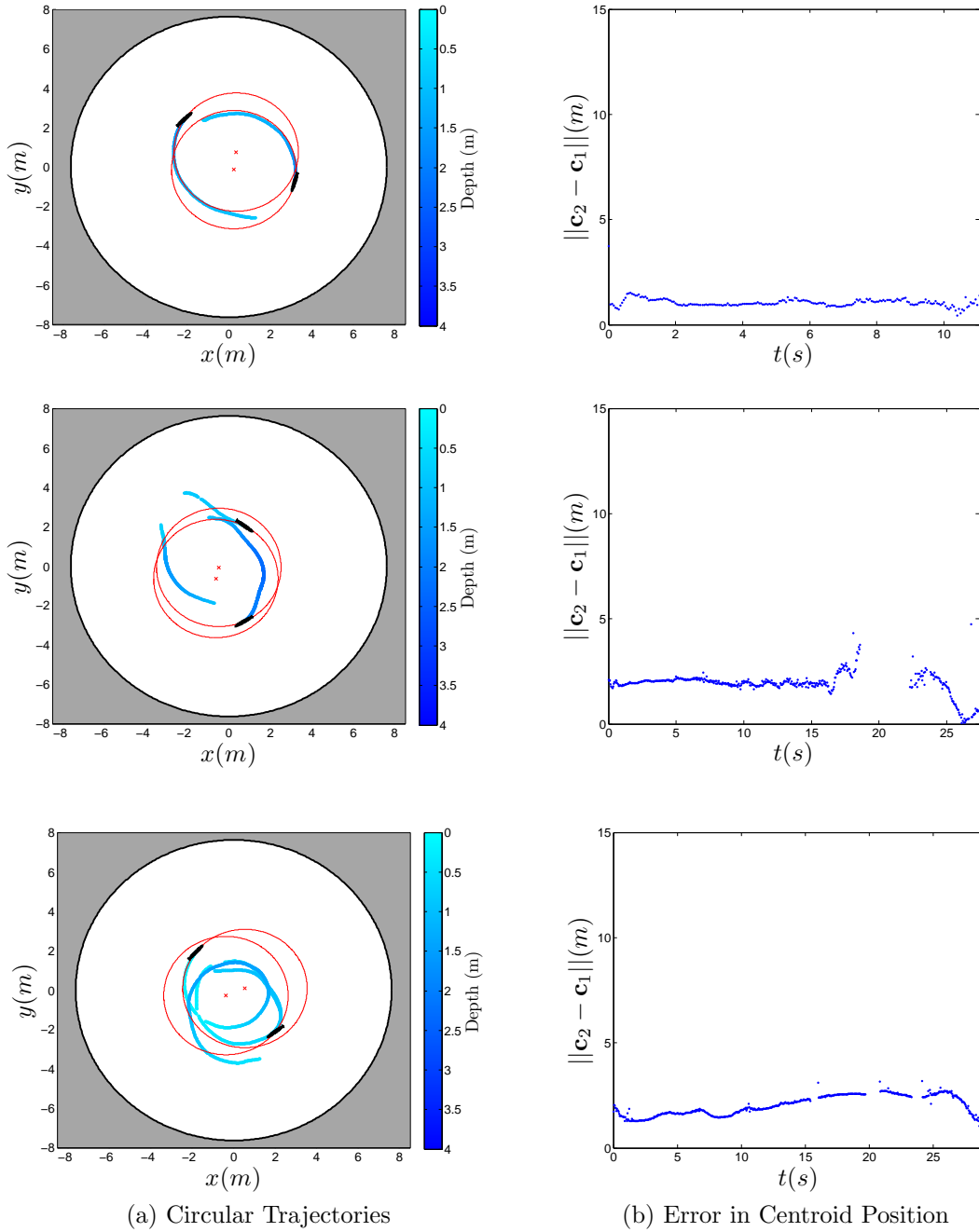


Figure 5.10: Experimental test runs of two submarines performing the circular control law.

are rotating in the correct direction and the centroid difference doesn't appear to be growing. These findings give us reason to think that these trajectories are still feasible, but may require additional modifications to the control algorithm.

### 5.3.3 Observer-Based Feedback Control Experiments

The testing of one and two vehicle systems above with the parallel (2.2) and circular (2.4) control laws have been implemented to show they can be achieved onboard a physical submarine. This testing was also completed to show that the control laws are feasible in a case when all the states are able to be measured. If the formation converges, we have reason to think that the observer-based feedback control algorithm can stabilize the formation as well.

For the parallel experiments described above, it has been realized that the submarines are a viable platform for implementation of the parallel control law. With this point in mind, the observer-based feedback control algorithm was implemented producing the following trajectory shown in Fig. 5.11. The addition of the observer appears to slightly degrade the performance when compared to the two submarine case. All in all, both submarines are traveling in, roughly, the same direction by the time they reach the edge of the tank.

The observer-based method was also implemented with the circular control law, with mixed results. Fig. 5.12 shows a test run of this case, where the performance is similar to the two submarine test of the circular control law. Again, we see each vehicle turning in the correct direction overall, but the difference in the

centroid appears to vary in time. Further study into this formation needs to be completed to provide more viable trajectories.

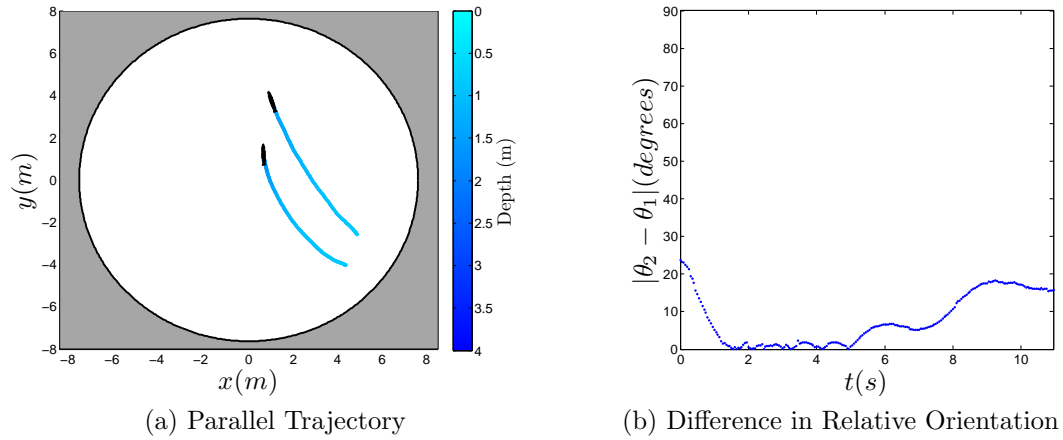


Figure 5.11: Experimental test run of two submarines performing the parallel control law using the observer-based feedback control algorithm.

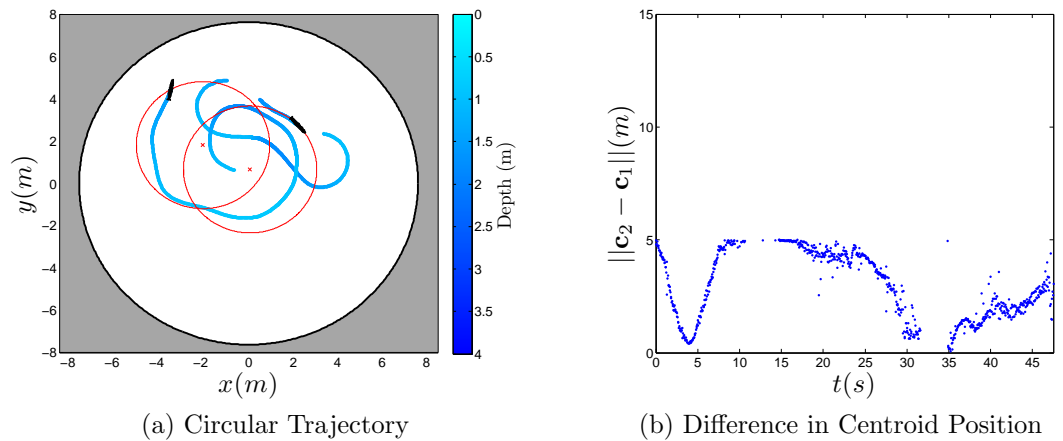


Figure 5.12: Experimental test run of two submarines performing the circular control law using the observer-based feedback control algorithm.

With all experimental tests completed and graphed, we conclude that a single submarine performing the parallel or circular control law with a virtual vehicle is a valid option for implementation on similar vehicles. In both cases, performance of the desired motion was consistently achieved with varying initial conditions. As for

multi-vehicle testing, we conclude that the parallel formation is a valid option for implementation with and without the observer. Results have indicated a slight loss of performance, as the complexity of the algorithm increases; however, the overall behavior can still be extracted. For circular formations, further research needs to be conducted with regard to the combination of vehicle dynamics and control. Finally, current results, although we are unable to validate these control algorithms, do indicate that the formation is worth further examination due to the successful virtual vehicle case.

## Chapter 6

### Conclusion & Future Work

#### 6.1 Conclusion

This paper describes an observer-based feedback control algorithm to stabilize parallel and circular formations. The proposed algorithm is theoretically justified for a second-order vehicle model, and simulations illustrate convergence to the desired formation. In addition, the cooperative control algorithms are extended to a three-dimensional rigid-body submarine model that obeys Euler's laws. Simulations using this model reinforce the theoretical results obtained by the idealized version. A laboratory scale testbed of underwater vehicles is also described in detail along with corresponding experimental results. Test runs using a virtual vehicle validate the parallel and circular control laws' ability to stabilize to a desired formation. Multi-vehicle testing of the cooperative control algorithms is also presented.

#### 6.2 Future Work

Throughout this paper, we analyzed collective control algorithms on a simplified vehicle model. Using this framework, a generic algorithm can be designed and applied to a variety of vehicles which mimic the behavior of the model. This control design process excludes the specific vehicle dynamics which ultimately determine

how the vehicle will operate autonomously. Although this concept is addressed by making modifications to the control law, designing the control around a specific model should also be researched. It is our hope that research in this area could produce a more stable version of the cooperative control algorithm with better overall performance.

In addition to this task, implementation of control has assumed that our sensors have zero noise. In general, this is not true because every sensor contains some inherent noise and may even be biased to some degree. This problem should be addressed in a stochastic formulation to describe how noise influences the vehicle's performance.

Also, consider the linear estimator that was used in our research to determine the relative velocity from one vehicle to another. Although the implementation of this estimator is straight-forward, it comes at a cost. This paper has indicated that the time-varying perturbation of this particular estimator greatly influences the stability of the system. Other estimation techniques for determining relative velocity should be researched to determine if they provide improved results. More specifically, nonlinear estimators such as the extended Kalman filter, could offer better estimates since the relative velocity does not vary linearly.

Lastly, experimental results in this paper began with a single submarine and a virtual particle. Tests were extended to the case where two submarines performed the cooperative motion. Future work should involve the implementation of control on larger groups of submarines as well as other platforms that can operate outside the testing facility. Vehicles fitting this profile can be used to demonstrate the value

of performing autonomous collective behaviors.

## Bibliography

- [1] Ardu-imu: Arduino based IMU & AHRS. <http://code.google.com/p/ardu-imu/wiki/Home>, July 2011.
- [2] Yongcan Cao, Wei Ren, and Ziyang Meng. Decentralized finite-time sliding mode estimators and their applications in decentralized finite-time formation tracking. *Systems and Control Letters*, 59(9):522–529, 2010.
- [3] Wei Ding, Gangfeng Yan, and Zhiyun Lin. Collective motions and formations under pursuit strategies on directed acyclic graphs. *Automatica*, 46(1):174–181, 2010.
- [4] A. J. Healey. Application of formation control for multi-vehicle robotic minesweeping. *Proceedings of the 40th IEEE Conference on Decision and Control*, 2:1497–1502, Orlando, Florida, 2001.
- [5] S. Hernandez and D. A. Paley. Three-dimensional motion coordination in a spatiotemporal flowfield. *IEEE Transactions on Automatic Control*, 55(12):2805–2810, 2010.
- [6] C H Hsieh, D Marthaler, B Q Nguyen, D J Tung, A L Bertozzi, and R M Murray. Experimental validation of an algorithm for cooperative boundary tracking. *Proceedings of the American Control Conference*, 2:1078–1083, 2005.
- [7] N. J. Kasdin and D. A. Paley. *Engineering Dynamics: A Comprehensive Introduction*. Princeton University Press, 1st. edition, 2011.
- [8] H. Khalil. *Nonlinear Systems*. Prentice Hall, Upper Saddle River, NJ 07458, 3rd. edition, 2002.
- [9] Daniel J. Klein, Patrick K. Bettale, Benjamin I. Triplett, and Kristi A. Morgansen. *Autonomous underwater multivehicle control with limited communication: Theory and experiment*. 2008.
- [10] Naomi Ehrich Leonard, Derek A. Paley, Francois Lekien, Rodolphe Sepulchre, David M. Fratantoni, and Russ E. Davis. Collective motion, sensor networks, and ocean sampling. *Proceedings of the IEEE*, 95(1):48–74, 2007.
- [11] Po-Hsiung Lin. The first successful typhoon eyewall-penetration reconnaissance flight mission conducted by the unmanned aerial vehicle, aerosonde. *Bulletin of the American Meteorological Society*, 87(11):1481–1483, 2006.
- [12] R. Mellish, S. Napora, and D. A. Paley. Backstepping control design for motion coordination of self-propelled vehicles in a flowfield. *International Journal of Robust and Nonlinear Control*, 21(12):1452–1466, 2011.

- [13] R. Mellish and D. A. Paley. Motion coordination of planar rigid bodies. *To appear in IEEE Conference on Decision and Control*.
- [14] R. C. Nelson. *Flight Stability And Automatic Control*. McGraw-Hill, 2nd. edition, 1998.
- [15] D. A. Paley and C. Peterson. Stabilization of collective motion in a time-invariant flowfield. *AIAA Journal of Guidance, Control, and Dynamics*, 32(3):771–779, 2009.
- [16] C. Peterson and D. A. Paley. Multi-vehicle coordination in an estimated time-varying flowfield. *AIAA Journal of Guidance, Control, and Dynamics*, 34(1):177–191, 2011.
- [17] D. O. Popa, A. C. Sanderson, R. J. Komerska, S. S. Mupparapu, D. R. Blidberg, and S. G. Chappel. Adaptive sampling algorithms for multiple autonomous underwater vehicles. *Autonomous Underwater Vehicles*, pages 108–118, 2004.
- [18] Endurance R/C. Endurance R/C - PCTx - PC to transmitter interface. <http://www.endurance-rc.com/pctx.php>, July 2011.
- [19] Endurance R/C. Optical motion capture - accurate tracking of any kind of motion. <http://www.qualisys.com>, July 2011.
- [20] M. Rubenstein and R. Nagpal. Kilobot: A robotic modules for demonstrating collective behaviors. *Proceeding of the IEEE Conference on Robotics and Automation*, Anchorage, Alaska, 2010.
- [21] R. Sepulchre, D. A. Paley, and N. Leonard. Stabilization of planar collective motion: All-to-all communication. *IEEE Transactions on Automatic Control*, 52(5):811–824, 2007.
- [22] R. Sepulchre, D. A. Paley, and N. E. Leonard. Stabilization of planar collective motion with limited communication. *IEEE Transactions on Automatic Control*, 53(3):706–719, 2008.
- [23] Housheng Su, Xiaofan Wang, and Zongli Lin. Flocking of multi-agents with a virtual leader. *IEEE Transactions on Automatic Control*, 54(2):293–307, 2009.
- [24] L. Techy, D. A. Paley, and C. A. Woolsey. UAV coordination on convex curves in wind: An environmental sampling application. *Proceedings of the European Control Conference*, pages 4967–4972, Budapest, Hungary, 2009.
- [25] L. Techy, C. A. Woolsey, and D. G. Schmale. Path planning for efficient UAV coordination in aerobiological sampling missions. *Proceedings of the 47th IEEE Conference on Decision and Control*, pages 2814–2819, Cancun, Mexico, 2008.